

W84-19470

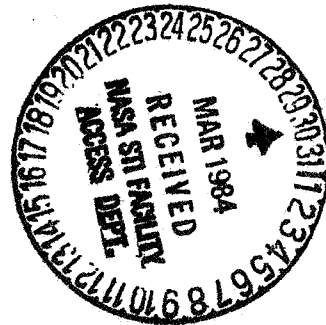
NASA TECHNICAL MEMORANDUM

NASA TM -77396

FLOW PROCESSES IN OVEREXPANDED CHEMICAL ROCKET  
NOZZLES. PART 1: FLOW SEPARATION

/ Robert H. Schmucker

Translation of "Strömungsvorgänge beim Betrieb Überexpandierter  
Duessen Chemischer Reketentriebwerke. Teil 1: Strömungsablösung,"  
Technische Universität, Munich (West Germany), Lehrstuhl für  
Raumfahrttechnik. Report Number TUM-LRT-TB-7 and NASA-CR-  
143044, July 3, 1973, pp 1-60.



NATIONAL AERONAUTICS AND SPACE ADMINISTRATION  
WASHINGTON, DC 20546 JANUARY 1984

## STANDARD TITLE PAGE

1. Report No. NASA-77396	2. Government Accession No.	3. Recipient's Catalog No.	
4. Title and Subtitle Flow processes in overexpanded chemical rocket nozzles. Part 1; Flow separation		5. Report Date January 1984	6. Performing Organization Code
7. Author(s) Robert H. Schmucker		8. Performing Organization Report No.	10. Work Unit No.
9. Performing Organization Name and Address Leo Kanner Associates Redwood City, CA 94063		11. Contract or Grant No. NASW-3541	13. Type of Report and Period Covered Translation
12. Sponsoring Agency Name and Address National Aeronautics and Space Admin. Washington, D.C. 20546		14. Sponsoring Agency Code	
15. Supplementary Notes "Strömungsvorgänge beim Betrieb Überexpandierter Düsen Chemischer Raketentriebwerke. Teil 1: Strömungsablösung," Technische Universität, Munich (West Germany), Lehrstuhl für Raumfahrttechnik, Report Number TUM-LRT-TB-7 and NASA-CR-143044, July 3, 1973, pp 1-60 (N75-26011)			
16. Abstract An investigation was made of published nozzle flow separation data in order to determine the parameters which affect the separation conditions. A comparison of experimental data with empirical and theoretical separation prediction methods leads to the selection of suitable equations for the separation criterion. The results were used to predict flow separation of the main space shuttle engine.  Sponsored by NASA, U.S. Academy of Sciences and Deutsche Forschungsgemeinschaft.			
17. Key Words (Selected by Author(s))		18. Distribution Statement Unclassified Unlimited	
19. Security Classif. (of this report) Unclassified	20. Security Classif. (of this page) Unclassified	21. No. of Pages	22.

## FOREWORD

The investigations on "Flow Processes in Overexpanded Chemical Rocket Nozzles" were conducted from March 1972 until February 1973 within the framework of the NRC Resident Research Associateship Program of the National Academy of Sciences (USA) in the Astronautics Laboratory of the George C. Marshall Space Flight Center of NASA (NASA-MSFC), Huntsville, Alabama, USA. My gratitude for their support and encouragement is due to Mr. C.R. Bailey, Scientific Advisor, K.W. Gross, H.G. Paul, Division Chief, and D. Pryor.

Since March 1973 these investigations have been supported by the German Forschungsgemeinschaft (DEG).

The result of the work is presented in three reports from the Lehrstuhl für Raumfahrttechnik of the TUM:

Flow Processes In Overexpanded Chemical Rocket Nozzles

Part 1: Flow Separation

Part 2: Side Forces due to Asymmetrical Separation \*

Part 3: Methods for Specific Flow Separation and Latéral Force Reduction.

\*Translator's Note: Available in translation as NASA TM-77395.

## TABLE OF CONTENTS

	Page
Foreword	ii
List of Symbols	iii
Summary	1
1. Introduction	2
2. The Process of Flow Separation	3
2.1 Pressure Distribution in a Laval Nozzle	3
2.2 Flow Separation Process	8
2.2.1 Pure Flow Separation	8
2.2.2 Separation and Recovery of the Flow	12
2.2.3 J-2 Separation Phenomena	13
2.3 Measurement of Separation	23
2.4 Beginning of Separation	25
2.5 Separation Criterion	26
3. Experimental and Theoretical Results of Flow Separation	27
3.1 Experimental Separation Results	27
3.1.1 Published Experimental Data	27
3.1.2 Methods of Graphic Representation	29
3.1.3 Compilation of the Separation Data on Chemical Rocket Engines	30
3.1.4 The Influence of Various Parameters on the Separation Behavior	31
3.1.5 Summary of Experimental Separation Results	36
3.2 Experimental Separation Criteria	36
3.3 Theoretical Calculation of the Separation	39
3.3.1 Overview of the Most Important Flow Separation Theories for Rocket Nozzles	39
3.3.2 Separation Theory of L. Crocco and R. Probstein [8]	40
References	44
Appendix: Prediction of Separation for the Space Shuttle Main Engine	48

## List of Symbols

### 1. Latin letters

F	Thrust
K	Constant
I	Pulse
l	Length
m	Mass
M	Mach number
p	Pressure
r	Radius
t	Time
T	Temperature
u	Velocity
y	Coordinate perpendicular to the nozzle wall

### 2. Greek letters

$\gamma$	Isentropy exponent
$\delta$	Boundary layer thickness
$\delta^*$	Compression thickness
$\epsilon$	Area ratio
$\theta$	Nozzle angle
$\Theta$	Pulse thickness
$\rho$	Density

### 3. Indices

a	Environ
c	Combustion chamber
CL	Crocco-Lees
CP	Crocco-Probstein
e	Nozzle end
i	Starting point of the recompression zone
p	Plateau point

r Rounding  
s Separation  
sc Separation criterion  
t Throat  
vac Vacuum  
w Wall

## SUMMARY

In the design of a rocket motor to be operated in alternating counter-pressure, the condition "no flow separation" plays an important role. This requires a corresponding specification of the nozzle wall-pressure distribution. In order to do this, several effects of multi-dimensional nozzle flow are treated and the various phenomena of flow separation in nozzles are described and compared.

An investigation of the various published flow separation data permits the specification of various parameters which affect the separation condition. A comparison of experimental data with empirical and theoretical separation prediction methods leads to the choice of suitable equations for the separation criterion. The results are applied to the flow separation prediction of the space shuttle main engine.

## 1. Introduction

In the design of a rocket motor to be operated inside the earth's atmosphere, the potential of flow separation in the nozzle plays an important role. This condition can occur during the burn periods of an engine whose nozzle is designed for great altitudes, without diffuser at low altitude, and results during the start-up, shut-down and excess propulsion-throttle phases. Under stationary conditions it is best to prevent flow separation since the location of the separation point of the flow is instable and leads to asymmetrical, oscillating forces which can damage the engine mountings [36].

Flow separation occurs in the supersonic portion of a rocket nozzle when the wall pressure at one point of the nozzle drops to 20 to 50 percent of the surrounding pressure due to over-expansion. Thus, the surface ratio of a given engine is chosen so that the flow does not separate under stationary operating conditions.

In an engine designed for a maximum power output in a vacuum which is to be ignited at sea-level\*, as is the case for the Space Shuttle main engine, the specification of the nozzle opening ratio is affected by two factors. The power output from a rocket engine increases with increasing opening ratio. Since the nozzle weight will also increase, there exists a point beyond which the power increase is eliminated by the increase in weight. The aspect of flow separation when operating at sea-level limits the opening ratio as well. Thus, an accurate design of the nozzle geometry is necessary. Too conservative a surface ratio leads to an undesired power loss.

Initial investigations on flow separation in nozzles were conducted by Büchner, Prandtl, Meyer, Flügel and Stanton and published by Stodola [25, 38, 40]. After World War II the increased research work in the area of rocket engines led to numerous investigations of this problem. Forster and Cowles at the California Institute of Technology undertook the first publicized hot-gas tests with a small nitric acid/anilin motor [13]. The result of this work was the separation condition that in an over-expansion to 40 percent of the surrounding pressure, the flow separates from the wall. This number is often called the "Summerfield Criterion" [3] and is today considered to be a conservative design value [3]. In the meantime, the results of numerous cold-gas tests and various hot-gas tests have been published which confirm the tendency of the measurements of Forster and Cowles.

---

\* Similar problems occurred for the Atlas Sustainer Motor and for the J-2 motor.

The rising performance requirements of rocket motors no longer permit the use of the simple Summerfield criterion for nozzle design. One is thus compelled to use more accurate predictions for the separation condition in nozzles in order to achieve a maximum engine power output.

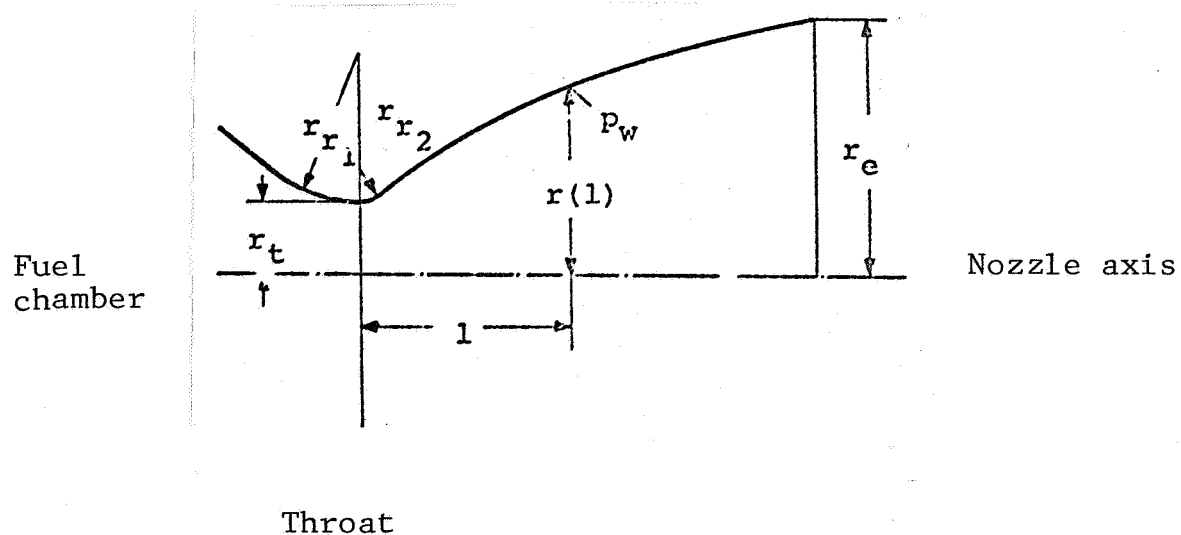
## 2. The Process of Flow Separation

For a treatment of the flow separation process, a description of experimentally observed phenomena is needed. The question of whether the flow separates in a nozzle depends essentially on the value of the nozzle wall-pressure reached as a function of the surrounding pressure. Thus the pressure distribution in a Laval nozzle will be investigated in more detail at first.

### 2.1 Pressure Distribution in a Laval Nozzle

Figure 1 presents a general Laval nozzle. The wall pressure  $p_w$  depends on the state of the combustion gas in the combustion chamber, the inlet and outlet conditions in the throat, expressed by the radii of curvature  $r_{r1}$  and  $r_{r2}$ , the local opening ratio  $\epsilon$  and the nozzle contour. In this case the opening ratio is:

$$\epsilon = \left(\frac{r(l)}{r_t}\right)^2 \quad (1)$$



Normally, to simplify the calculation, a one-dimensional flow is assumed as is a constant pressure over the nozzle cross-section [3, 42]. For an ideal gas with the isentropic exponent  $\gamma$  the relationship between the wall pressure, the chamber pressure  $p_c$  and the opening ratio is obtained as:

$$\epsilon = \frac{\gamma^{0.5} \left(\frac{2}{\gamma+1}\right)^{\frac{\gamma+1}{2(\gamma-1)}}}{\left(\frac{p_w}{p_c}\right)^{\frac{1}{\gamma}} \left\{ \frac{2}{\gamma-1} \left(1 - \left(\frac{p_w}{p_c}\right)^{\frac{\gamma-1}{\gamma}}\right) \right\}^{0.5}} \quad (2)$$

Thus the wall pressure, normed with the fuel-chamber pressure, can be determined for any cross-section ratio. For long nozzles with small divergence angle and large inlet radius, these values agree well with the experimental data [13, 33].

But if the divergence angle is greater than  $10^\circ$  or if nozzles with curved contours are used, then greater deviations result from the one-dimensional theory, since the pressure distribution is no longer constant over the cross-section. The one-dimensional theory then only gives the average ratios in the cross-section. The trend of the pressure distribution in the nozzle cross-section--whether the wall pressure is greater or smaller than the one-dimensional pressure--depends on the location of the cross-section relative to the throat and end cross-section. For an accurate calculation of the flow field in the nozzle, methods like the method of characteristics must be applied. In fig. 2 the wall pressure distribution in a bell nozzle of a LOX/LH<sub>2</sub> high-pressure engine is shown. Along the axis is also the nozzle contour corresponding to the Space Shuttle main engine. In a calculation of the wall pressure, the following points were taken into account [17]:

- o Two-dimensional rotation-symmetric flow field and relaxation of the combustion gas (kinetic relaxation)
- o Mixing ratio distribution over the injector (20 flow tubes)
- o Wall temperature distribution and change of the real contour through compression thickness of the boundary layer
- o Increase in enthalpy of the fuels before injection due to heat addition during cooling.

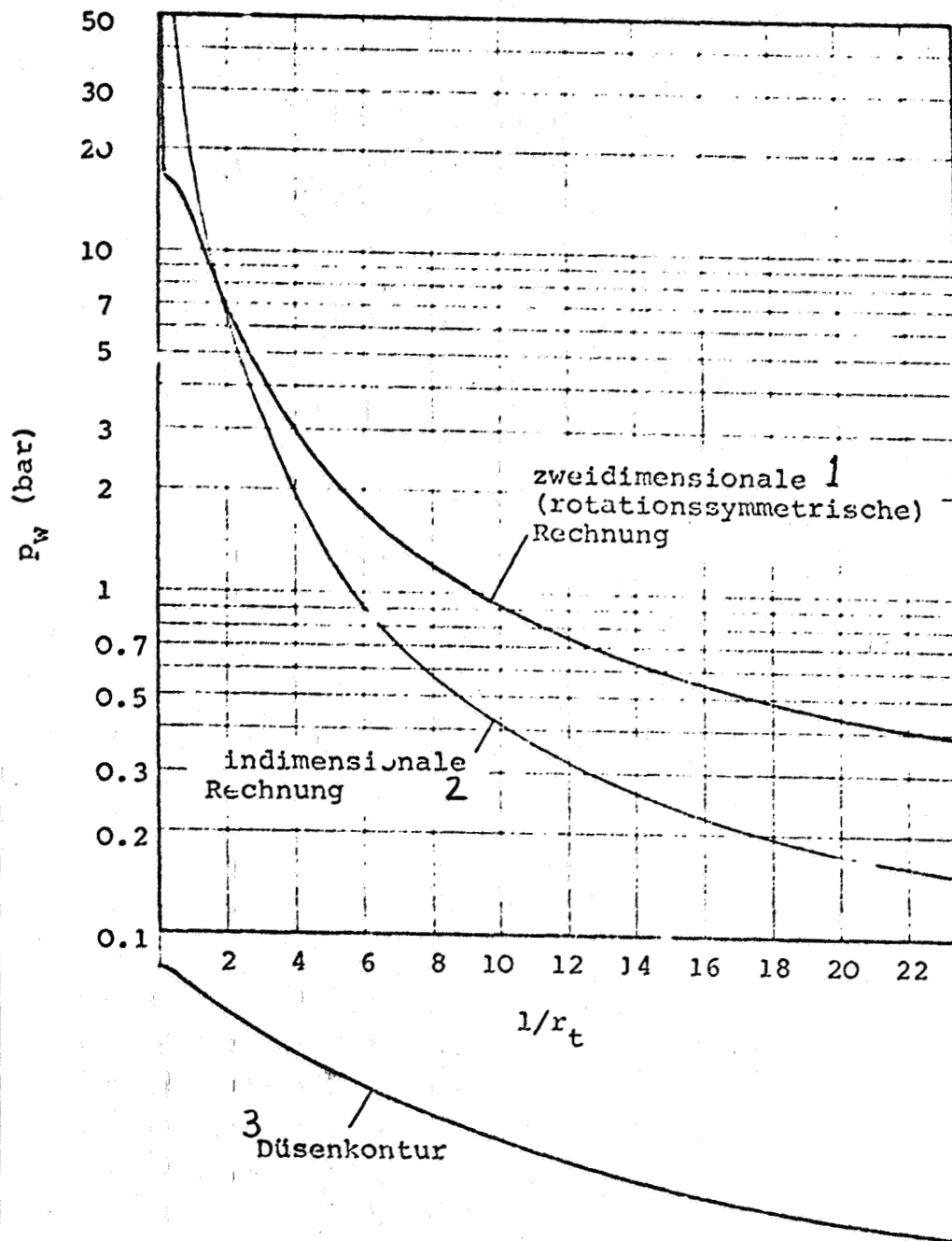


Fig. 2: Wall Pressure Distribution in the Bell Nozzle of an LOX/LH<sub>2</sub> High-Pressure Engine Compared with the One-Dimensional Pressure Values (Contour and Data are that of the Space Shuttle Main Engine:  $p_c = 205$  bar,  $F = 2170$  kN,  $\epsilon = 77.5$ , length 80% of a 15° plug nozzle,  $r_{r1}/r_t = 1$ ,  $r_{r2}/r_t = 0.392$ ) [17, 29].

Key: 1-two-dimensional (rotation-symmetrical) calculation  
 2-one-dimensional calculation  
 3-nozzle contour

As a comparison to this nearly "real" pressure distribution, the one-dimensional pressure values are also listed. It turns out that in the throat region the multi-dimensional pressure drops off much faster than the one-dimensional calculation would indicate. The severe change in the pressure gradient when moving from the throat rounding to the parabolic contour, leads to weak compression jolts. In the wide part of the nozzle, the "real" pressure is about 2 to 3 times greater than the one-dimensional. The wall pressure at the nozzle end corresponds to the one-dimensional pressure at a surface ratio of about 40.

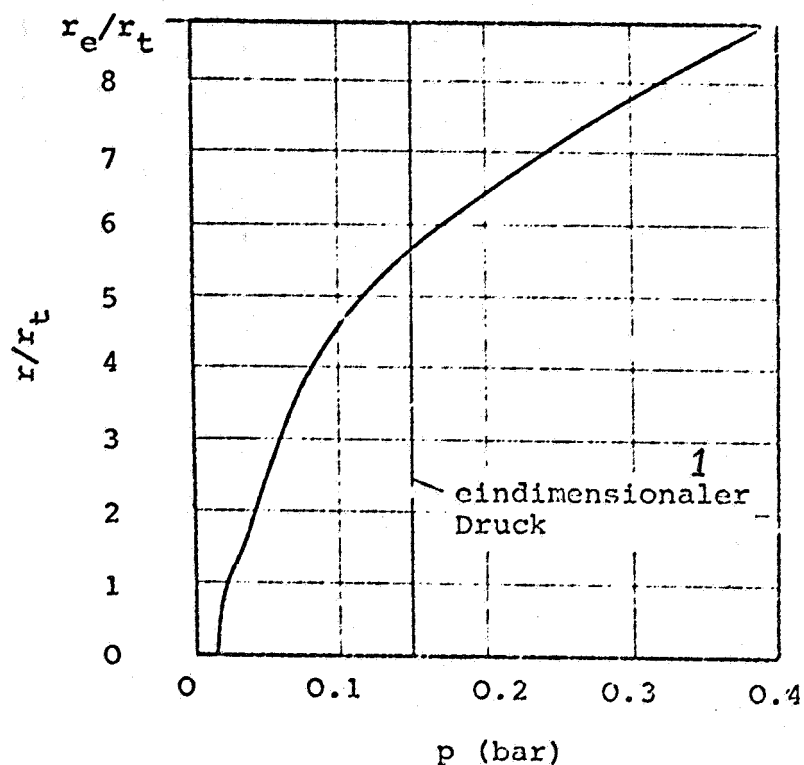


Fig. 3: Pressure Distribution in the End Cross-Section  
(Nozzle Contour from fig. 2)

Key: 1-one-dimensional pressure

Since the wall pressure is considerably greater than the average pressure, the pressure of the core flow must be much less. Figure 3 shows the pressure distribution in the end cross-section of the nozzle of figure 2. The shape of the pressure distribution near the axis is emphasized by the mixing-ratio variation at the injection head.

The pressure distribution at the wall can be influenced by a change in nozzle contour at constant length and constant expansion ratio. In figure 4 various possible contours and the wall pressure distribution for doing this, are shown for a nozzle

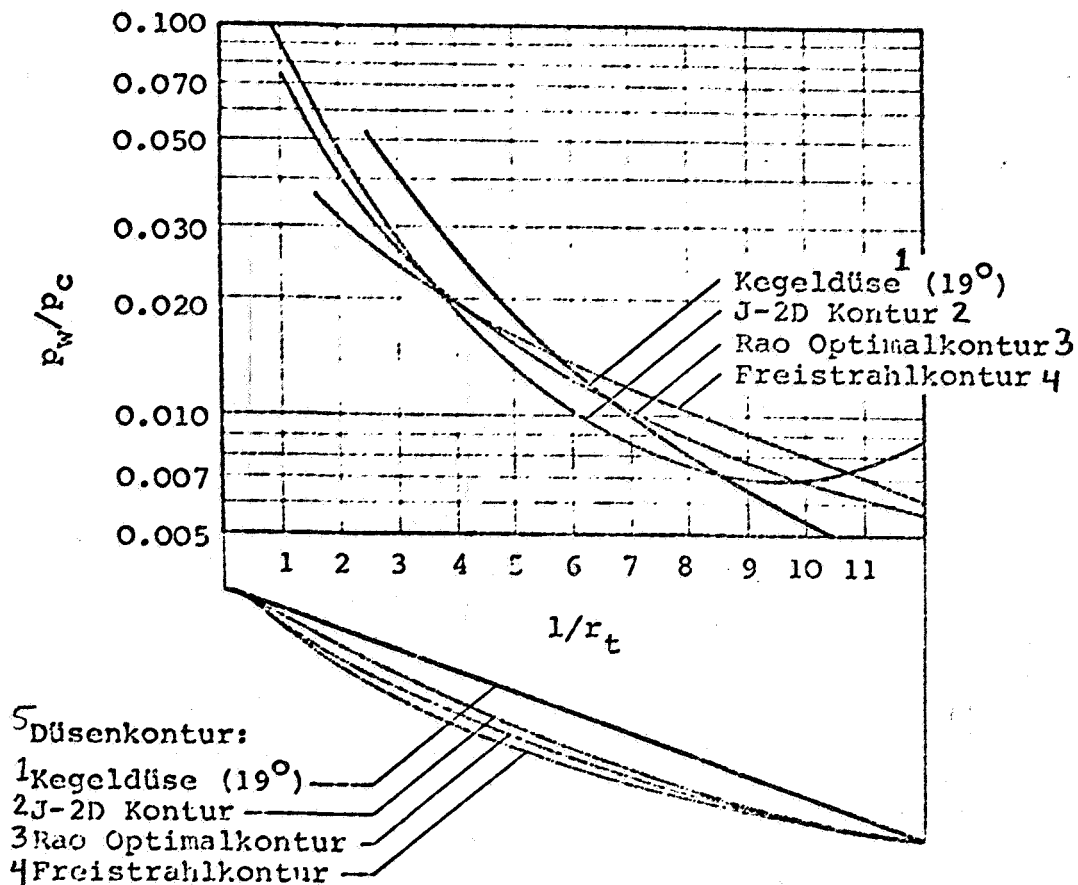


Fig. 4: Wall Pressure Distribution and Nozzle Contour (Nozzle Length 75% of a 15° Plug Nozzle,  $\epsilon = 27.5$ ,  $\gamma = 1.2$ )

Key: 1-plug nozzle 2-J-2D contour 3-Rao optimum contour  
4-free jet contour 5-nozzle contour

with 75% of the length of a plug nozzle of 15° and an area ratio of 27.5. The plug nozzle gives the lowest nozzle end-pressure. In operation behind the nozzle throat, the wall pressure is greater than in a bell nozzle, since the local cross-section ratio is even smaller. Proceeding from an optimum contour (Rao optimum contour) which gives the greatest-possible thrust coefficient in a vacuum for this length and opening ratio, the shape can be changed so that the wall pressure increases in the end cross-section. This increase is obtained through a greater inward curvature of the wall. Although the end-pressure is increased, the thrust coefficient decreases slightly [27]. Through suitable change of the wall curvature radius along the nozzle axis, a pressure increase can be achieved in spite of an expanded contour (J-2D contour).

Therefore, a multi-dimensional expansion must always be used as a starting point in the investigation of separation behavior. The use of one-dimensional computed wall-pressure values can invalidate the results [33].

## 2.2 Flow Separation Process

### 2.2.1 Pure Flow Separation

The flow field in an over-expanded nozzle with pure flow separation and the pertinent wall-pressure distribution are presented in figure 5.\* This type of flow separation is most frequently observed for chemical rocket engines.

Proceeding from the combustion chamber, the gas expands in the nozzle. If the surrounding pressure is negligible, then the pressure distribution does not change. This pressure should thus be designated as the "vacuum wall pressure." Due to the viscosity a boundary layer forms on the wall. Since this is normally turbulent in rocket engines, only the turbulent flow separation shall be discussed.

If the surrounding pressure is higher than the nozzle end pressure, then a compression shock is needed to compress the jet to the outside pressure. The boundary layer can only exist in a certain pressure difference, above which it separates. In this case the gas jet initially expands in the manner described above up to a point *i* at which the separation process begins due to a severe pressure increase. The boundary layer thickens and a slanting compression shock is generated which extends deep into the boundary layer. Within a few boundary-layer thicknesses the pressure rises almost to the surrounding pressure and the boundary layer separates off. The separation angle in most experiments is constant at about  $13.5^\circ$  [20]. Downstream the wall pressure increases only a little after the sharp pressure increase, until it almost reaches the surrounding pressure.

This classical picture of flow separation in an over-expanded supersonic nozzle permits the definition of four different (time-averaged) points:

- i*: At point *i* the first deviation from the vacuum wall-pressure profile is found. At this point the re-compression of the flow begins, but no separation occurs yet.

---

\*The wall pressure distribution, the characteristic points and the various spacings result as time averages of low-frequency wall pressure measurements. This data can be used for a description of the separation process and for the nozzle design.

High-frequency pressure measurements show however, that the separation point oscillates within the separation length. This behavior is discussed in section 2.2.3 and especially in [36] (part 2: Lateral Forces due to Asymmetrical Separation).

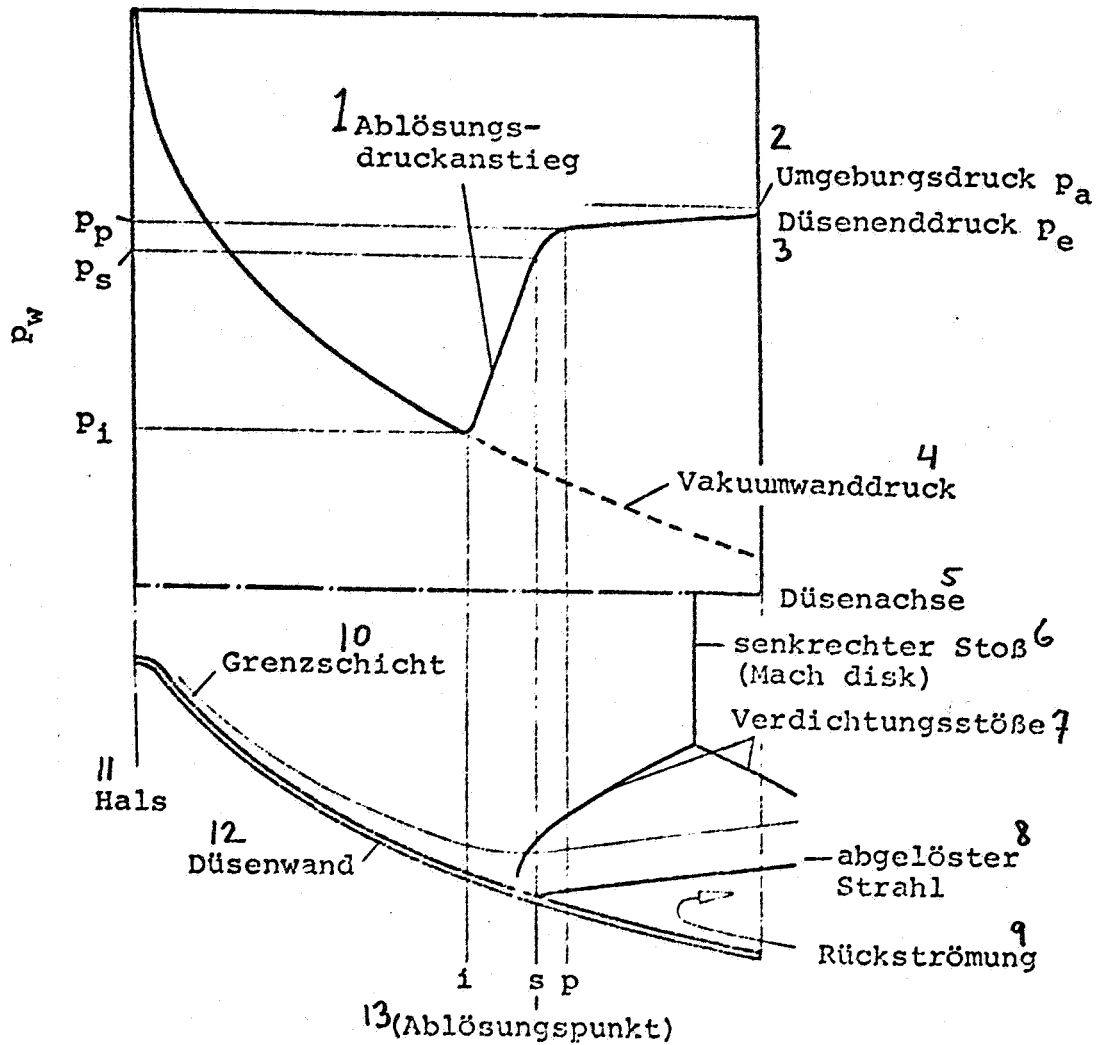


Fig. 5: Flow and Wall-Pressure Distribution in an Over-Expanded Nozzle with Pure Flow Separation.

- i Beginning of the separation region
- s Separation point
- p Plateau point

- Key:
- |                                   |                     |
|-----------------------------------|---------------------|
| 1-separation pressure increase    | 8-separated jet     |
| 2-surrounding pressure            | 9-back-flow         |
| 3-nozzle end-pressure             | 10-boundary layer   |
| 4-vacuum wall-pressure            | 11-throat           |
| 5-nozzle axis                     | 12-nozzle wall      |
| 6-perpendicular shock (Mach disk) | 13-separation point |
| 7-compression shock               |                     |

- s: The flow separates at point s. The location of this point can be determined in cold-gas tests with oil films etc. In hot-gas rocket tests, such methods cannot be applied; thus the actual separation point almost always cannot be determined. Only the deposition of soot [41] or condensation on the wall (see sec. 2.2.3) can provide any information. Between i and s the greatest part of the separation pressure-increase takes place. Cold-gas tests in wind tunnels with steps, incident compression shocks etc. show that more than 80% of the total pressure increase occurs in this region. The spacing between i and s is small and amounts to about 3 boundary-layer thicknesses in cold-gas tests [20]. The spacing presented in [29] of only one boundary-layer thickness deviates considerably from this and is somewhat questionable.
- p: At point p the steep pressure gradient of the separation region flattens out. This spot is called the plateau pressure point. The point p is somewhat difficult to define since the pressure gradient never disappears between i and the nozzle end. Between i and p the entire separation process takes place. The separation amounts to about 6 boundary-layer thicknesses [20, 29] and is called the separation length.
- e: In the region between the plateau pressure-point and the nozzle end cross-section, the final pressure increase occurs. The nozzle end-pressure is somewhat lower than the surrounding pressure, since the outside air is sucked in due to a back-flow. The pressure increase between p and e is affected by the nozzle shape. For normal nozzles, it is small and increases almost linearly between p and e. In the tests described in [25] with parabolic nozzles, a stronger pressure gradient is found near e and a detailed plateau point. This pressure distribution appears to be caused only by the type of plotting, since the pressure is illustrated not as a function of the nozzle length, but of the surface ratio. In a parabolic nozzle the increase in the surface ratio becomes increasingly smaller with decreasing distance from the nozzle end.

The location of the separation point depends on the combustion chamber and surrounding pressure. If the chamber or outside pressure is changed, then only the region of flow separation is shifted. Figure 6 shows the wall pressure measured for a plug nozzle with different surrounding pressures. The wall pressure is normed with the combustion-chamber pressure, since in the individual experiments, the same chamber pressure could not always be attained. The vacuum pressure profile is practically independent of the pressure within a broad range of chamber pressure in the normed case. If the surrounding pressure is much greater than the nozzle end-pressure, then the wall-pressure distribution described above sets in and the jet separates off far inside the

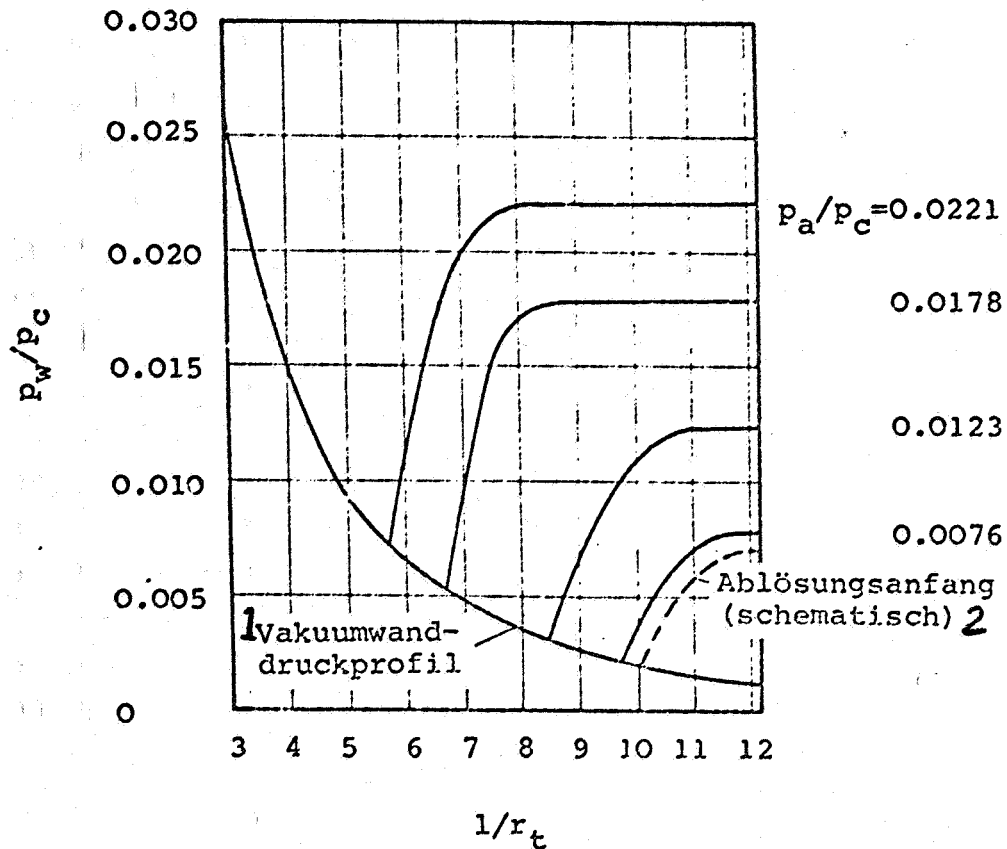


Fig. 6: Wall Pressure Distribution as a Function of the Throat Spacing for Different Pressure Relationships  $p_c/p_a$  [4].

Key: 1-vacuum wall-pressure profile  
2-beginning of separation (schematic)

nozzle. If the chamber pressure is increased or if the outside pressure is reduced, then the separation region shifts in the direction of the nozzle end. Since the boundary-layer thickness increases, the separation region and the pressure gradient decrease.

The location of the first pressure-increase point  $i$  is illustrated in fig. 7 as a function of the pressure relationship  $p_c/p_a$ . The distance from the nozzle end decreases continually until finally, the outside pressure and the nozzle end-pressure coincide.

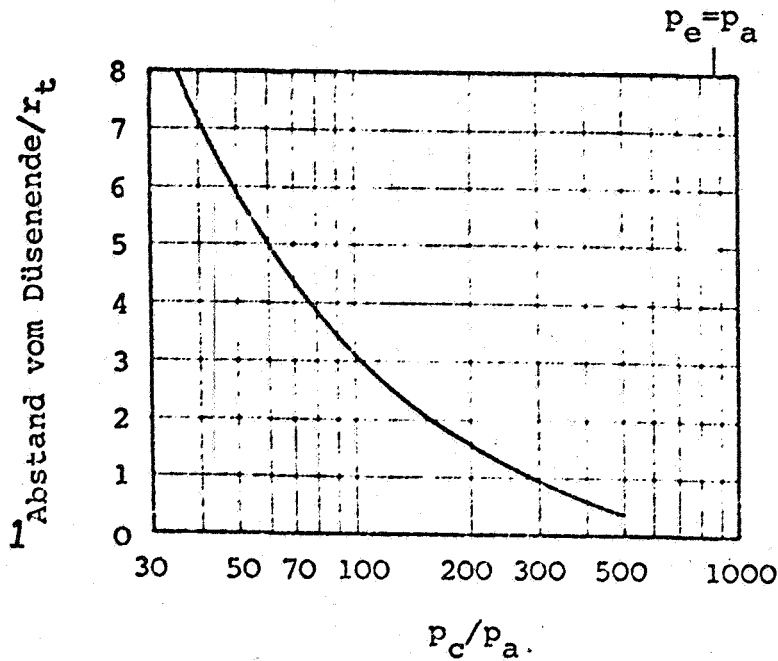


Fig. 7: Distance of the First Point of Pressure Increase  $l$  from the Nozzle End, Plotted Against the Pressure Ratio  $p_c/p_a$  [4]

Key:  $l$ —distance from the nozzle end

### 2.2.2 Separation and Recovery of the Flow

Normally after the separation of the flow there is no flow recovery. In [29, 39, 42] a wall-pressure profile is described which differs from that of pure flow separation. The gas jet expands in the nozzle at lower pressure values than for pure separation. The wall pressure in the separation region surpasses the surrounding pressure and then drops off to the outside pressure. In figure 8 a pressure measurement of this process is presented. In contrast to pure flow separation where the exhaust jet fills up only a part of the nozzle end cross-section, in the end cross-section no separation from the wall is observed.

This behavior of the nozzle which was already discovered by Stodola [38], is similar to the flow in supersonic tubes with compression shock [37]. Thus, a flow field can be defined which is seen in fig. 9. The sharp compression shock, generated in the separation region, is reflected at the perpendicular shock. The Mach disk fills almost the entire nozzle cross-section. The reflection of the shock causes a recovery of the flow so that the nozzle has full flow.

The few available data indicate that this phenomenon can occur primarily in small nozzles with low outlet angle. This configuration is similar to that of a cylindrical tube with supersonic velocity. In a small nozzle moreover, the boundary layer takes up relatively more space than in a large nozzle.

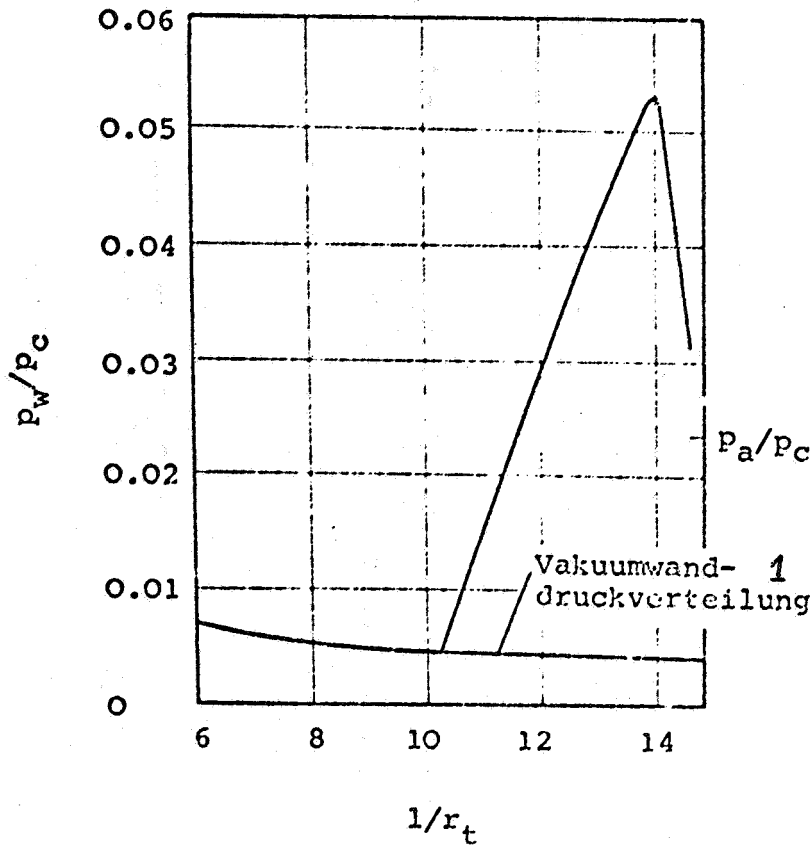


Fig. 8: Wall Pressure Distribution upon Separation and Recovery of the Flow (Cold Gas J-2 Nozzle,  $\epsilon = 40$  [39]).

Key: 1-vacuum wall-pressure distribution

### 2.2.3 J-2 Separation Phenomena

Low-frequency measurements of wall pressure in a circumferential direction in a 4-k  $H_2/LOX$  motor (NASA-MSFC) and soot deposits [41] show that in the case of pure separation, the separation line runs rather axis-symmetrical in a time-average.

The visual observations of the interior of the nozzle of J-2 engines gave a picture which deviates significantly from this. This optimistic description of the separation process is possible in a J-2 engine since the exhaust jet of an  $LH_2/LOX$  engine is transparent and cryogenic cooling of the nozzle leads to condensation on the wall. Instead of a smooth separation line, triangular-shaped tepees are observed which change position in the circumferential direction and along the nozzle axis at low frequency. Figure 10 presents a cross-section through a J-2 engine and these phenomena are illustrated schematically. This figure also indicates the camera position to observe the separation phenomena. Figure 11 shows a photograph of the nozzle interior with the significant phenomena also entered.

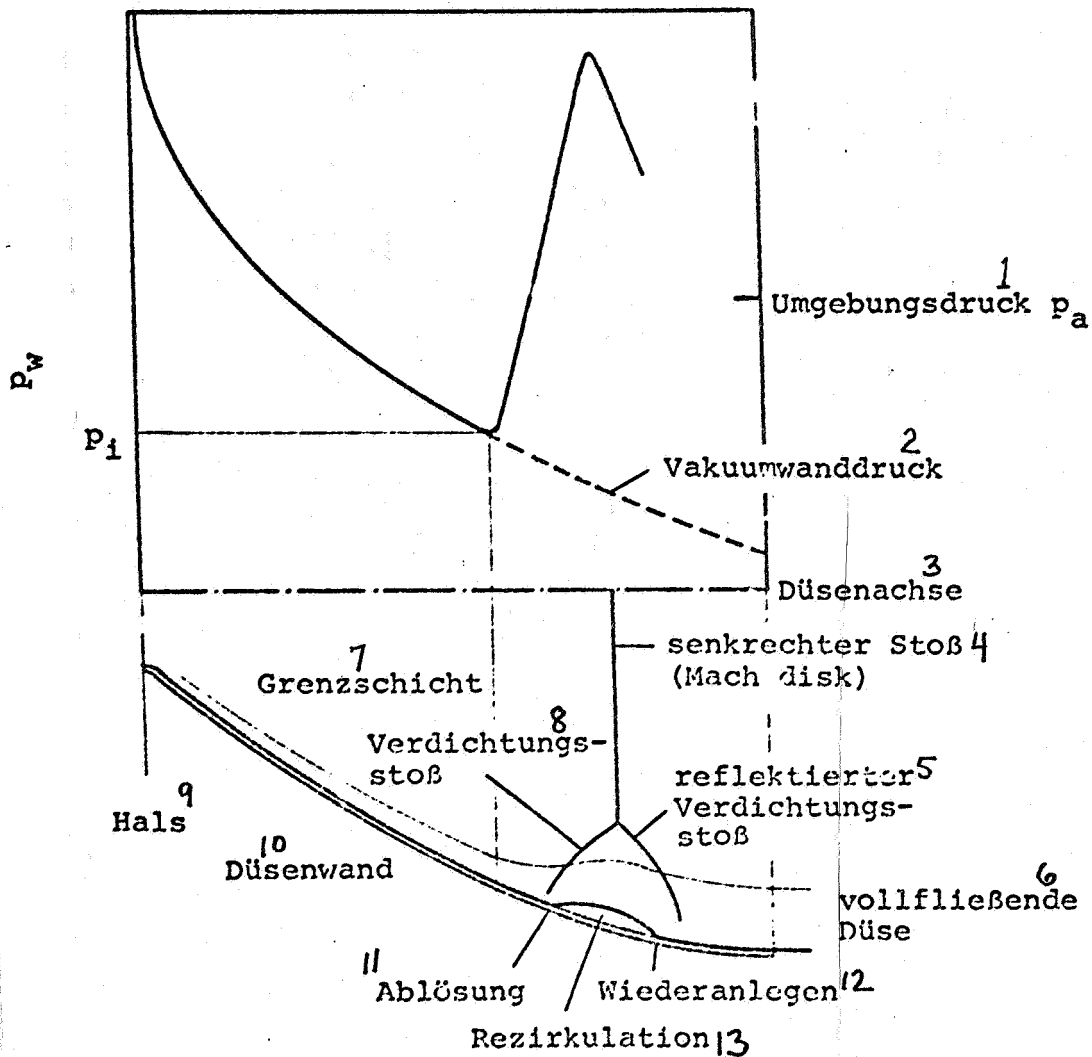


Fig. 9: Schematic of the Wall-Pressure Distribution and of the Flow Field in a Nozzle with Separation and Recovery

- |                                   |                              |
|-----------------------------------|------------------------------|
| Key: 1-surrounding pressure       | 7-boundary layer             |
| 2-vacuum wall pressure            | 8-compression shock          |
| 3-nozzle axis                     | 9-throat                     |
| 4-perpendicular shock (Mach disk) | 10-nozzle wall               |
| 5-reflected compression shock     | 11-separation                |
| 6-full-flowing nozzle             | 12-flow recovery to the wall |
|                                   | 13-recirculation             |

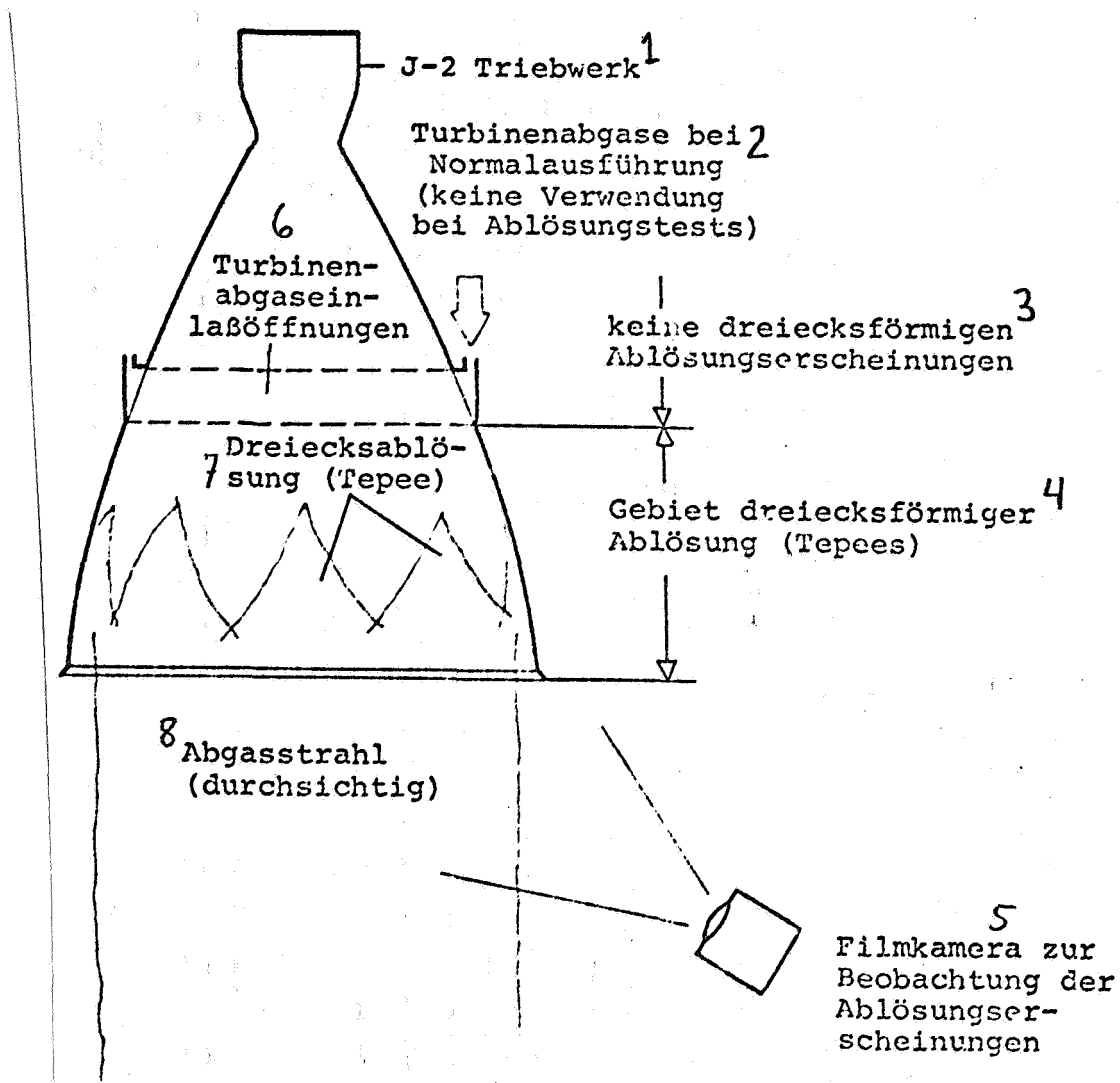


Fig. 10: Schematic Illustration of the J-2 Engine with the Observed Separation Phenomena

- |  |   |
|--|---|
| Key: 1-J-2 engine  | 5-film camera to observe the separation phenomena |
| 2-turbine exhaust of normal design (not used for separation tests) | 6-turbine exhaust inlet openings                  |
| 3-no triangular separation phenomena                               | 7-triangular separation (Tepee)                   |
| 4-region of triangular separation (Tepees)                         | 8-exhaust jet (transparent)                       |

The J-2 unit is a 1000 kN LH<sub>2</sub>/LOX engine whose combustion chamber and nozzle are made of 360 and 540 thin-wall tubes. At an area ratio of 12.5 (J-2D) the turbine exhaust is normally blown into the nozzle under normal operation. During the separation tests, the turbine gases were ejected to the outside through a tube to the side of the engine (fig. 11).

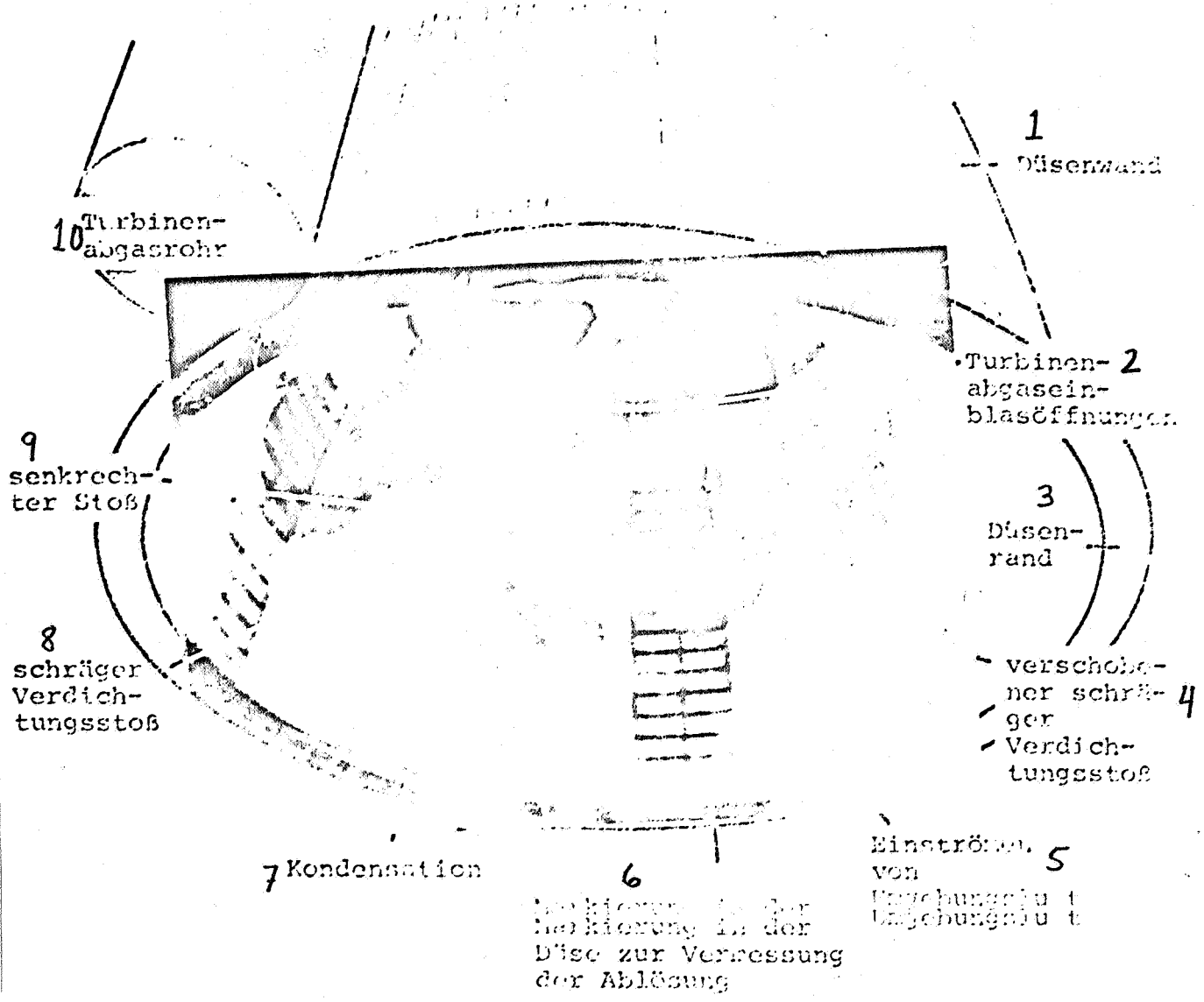


Fig. 11: Separation Phenomena in a J-2 Engine (Saturn S-II and S-IV Stage)

- |                                      |   |
|--------------------------------------|---|
| Key: 1-nozzle wall                   | 6-marking in the nozzle to measure the separation |
| 2-turbine exhaust inlet openings     | 7-condensation                                    |
| 3-nozzle edge                        | 8-slant compressing shock                         |
| 4-shifted, slanted compression shock | 9-perpendicular shock                             |
| 5-inflow of surrounding air          | 10-turbine exhaust tube                           |

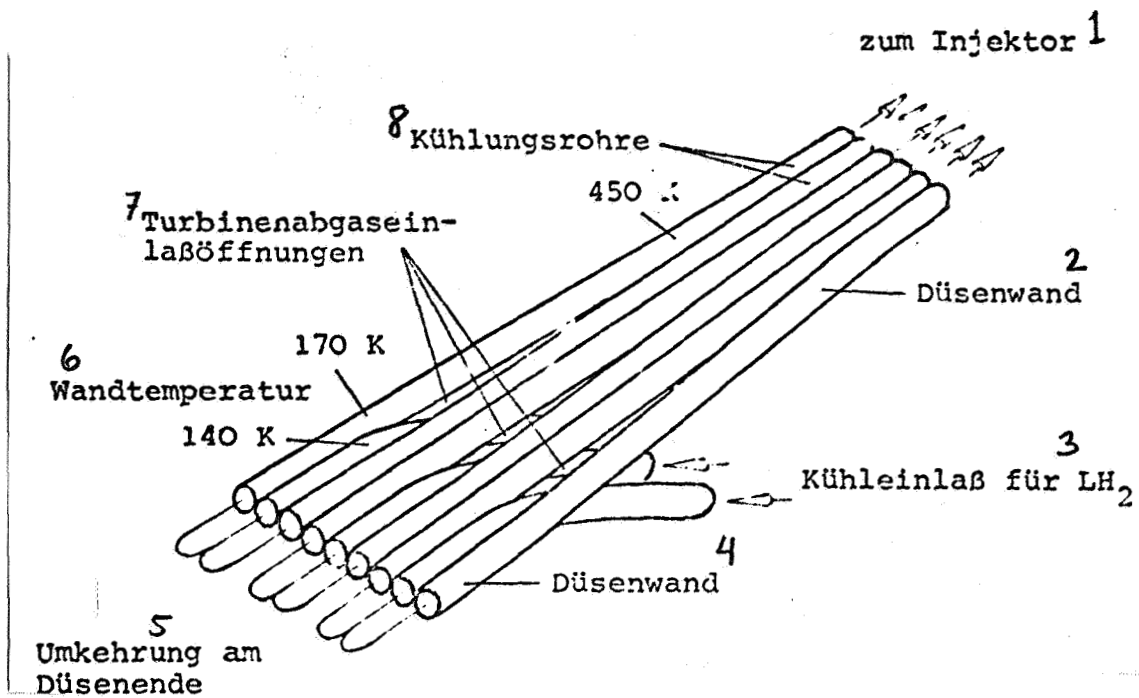


Fig. 12: Schematic of the Turbine Exhaust Blow-in Openings (Cat Eyes)

Key: 1-to the injector                      5-reversal at the nozzle end  
 2-nozzle wall                              6-wall temperature  
 3-cooling inlet for LH<sub>2</sub>                7-turbine exhaust inlet openings  
 4-nozzle wall                              8-cooling tubes

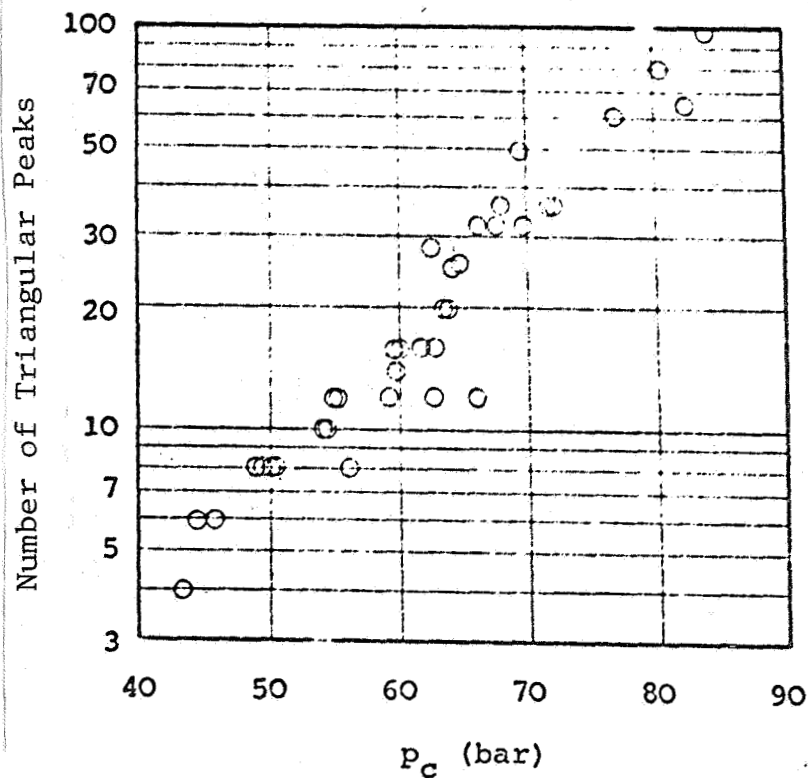


Fig. 13: Number of Triangular Peaks as a Function of the Chamber Pressure for J-2S Engine [12].

In figure 12 the turbine exhaust blow-in position is shown schematically. By increasing the number of tubelets from 360 to 540, triangular slits (Cat Eyes) result which interrupt the wall along a distance of about 10 cm. In several separation tests these openings were sealed with sheet-metal triangles and ablation material, without decisively changing the optical separation picture. In this turbine exhaust inlet region the wall temperatures change very much. They drop by about 300 K in the direction of the nozzle end; due to the feed of coolant the temperature in the circumferential direction is not constant (temperature calculation as per [27]). The temperature of the uncooled blow-in openings might reach 1000 K since several sheet-metal triangles sealing the openings were blown out during the tests.

The phenomena occurring in the different experiments (J-2S engine at Rocketdyne [12, 14], J-2D engine at NASA-MSFC) can be characterized as follows:

o Optical Separation Observations:

The triangular-shaped separation phenomena are only observed in the region between Cat Eyes and nozzle end. The suction of surrounding air, the condensation of water vapor on the nozzle wall and a wedge-shaped compression shock whose divergence angle increases in the direction of the nozzle end, are seen. For a fixed combustion chamber pressure, the triangular peaks extend only up to a certain maximum position in the nozzle. This distance depends on the combustion chamber pressure, just like the number of triangles. Figure 13 shows the number of tepees as a function of the chamber pressure.

The evaluation of high-speed film indicates that the phenomena occur periodically. If three sequential tepees are considered, then the middle triangle increases when the other two decrease, and vice-versa. The frequencies and shock life-span of these processes are presented in table 1:

Table 1: Frequency of Triangular Phenomena in the J-2S Nozzle [14]

Combustion chamber pressure (bar)	Mixing ratio LOX/LH <sub>2</sub>	Life-span (ms)	Frequency (Hz)
62 - 65	4.4 - 4.5	85 - 90	10.5 - 11
59 - 60	4.3	105	9.6
51 - 56	4.4 - 4.8	65 - 95	10.5 - 15

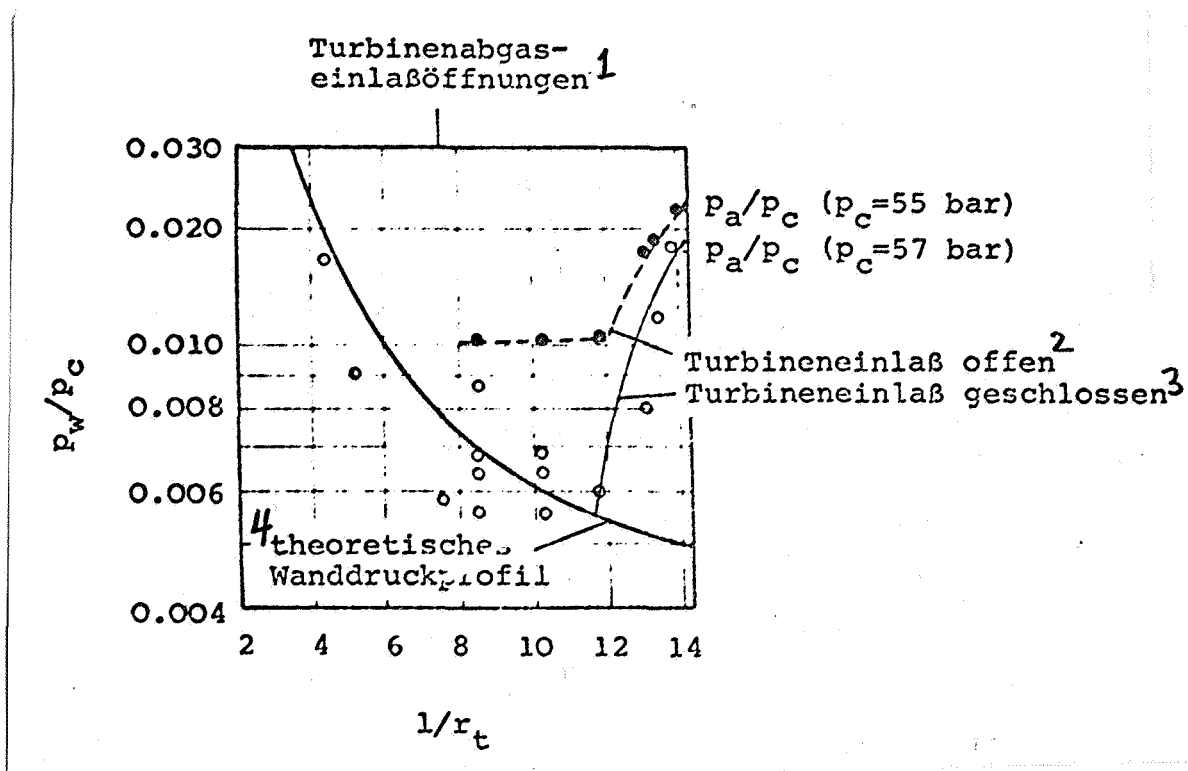


Fig. 14: Wall Pressure Measurements of the J-2S Experiments [12, 14]

----- Turbine inlet openings open  
 \_\_\_\_\_ " " " closed

Key: 1-turbine exhaust inlet openings    3-turbine inlet closed  
 2-turbine inlet open                    4-theoretical wall-pressure profile

o Measurements of Wall Pressure:

The measurements of wall pressure to determine the flow separation exhibit several anomalies. In the experiments where the turbine inlet is not closed, theoretical and experimental wall pressure do not agree. The experimental wall pressures are greater than the calculated ones; with decreasing chamber pressure, this difference increases. Tests with the same unit and closed turbine exhaust openings indicate a wall pressure which is less than the theoretical, however the measurement accuracy is not very great. Figure 14 shows the wall-pressure distribution of these tests. Some comments are in order for the pressure deviations. All model tests produce wall pressures which agree with theory; the J-2D NASA-MSFC measurements also lead to agreement between theory and experiment. Lower wall pressures than the theoretical are presented in [22] and are explained by compression shocks behind the throat.

One can attempt to explain the optical phenomena by high-frequency measurements of wall pressure. Figure 15 shows the chronological wall-pressure profile for rising combustion-chamber pressure during the start-up phase. Time is counted from the switch-on point.

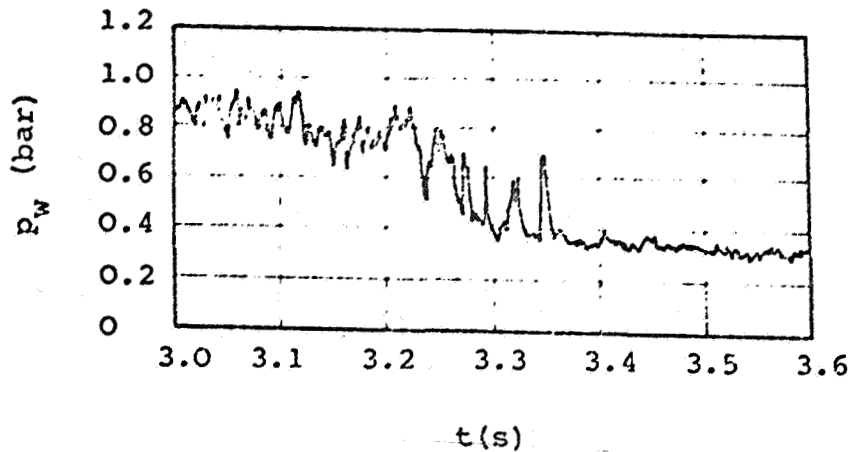


Fig. 15: High-Frequency Wall-Pressure Measurement During the Start-up Phase of the J-2D Engine (Wall Pressure and Contour see fig. 4:  $1/r_{t\text{meas. pt.}} = 7.8$ )

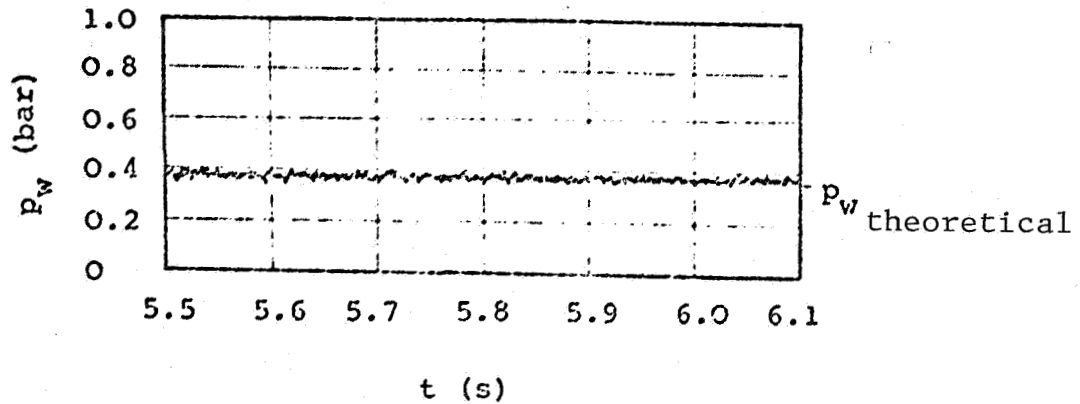


Fig. 16: Measurement of Wall Pressure During Operation of the J-2D Engine ( $1/r_t = 7.8$ ,  $p_c = 46$  bar)

The transition from separated flow to full-flowing nozzle shows up. Pumping off the measurement point occurs by oscillation and can be explained by vibrations of the separation point (see [36]). The low-frequency vibrations are at 30 Hz and do not correlate with the frequency of the tepees or engine structure vibrations. Wall pressures at other places and especially farther downstream ( $1/r_t = 8.2$  and  $1/r_t = 9.1$ ) show the same behavior. Although the film recordings show triangular separations which would have to lead to severe oscillations in the wall-pressure measurements, the amplitudes of the oscillations are only 0.03 bar. Figure 16 shows the wall-pressure profile of the above measurement point at a later time. The measurements of wall pressure show no evident correlation between pressure oscillations and triangular phenomena.

To clarify the optical phenomena and the wall-pressure anomalies found in the first J-2S tests, different interpretations were proposed which pertained primarily to the following points:

- o Correlation between injector and separation picture
- o Nozzle contour changes due to
  - o Pressure
  - o Temperature
  - o Vibrations
  - o Boundary layer
- o Three-dimensional boundary layer due to the tube construction of the nozzle wall
- o Disturbance of the wall contour due to
  - o Turbine inlet openings
  - o Wall temperature differences in the circumferential direction
- o Boundary layer changes due to
  - o Chemical reaction
  - o Laminarization
  - o Long separation region
- o Condensation shock at the wall due to subcooling.

Until now no final clarification of the optical phenomena and the wall-pressure behavior has been given. But the observed phenomena and the measurements of others lead to the following summary points:

- o The separation line oscillates asymmetrically within a certain region and can only be viewed as nearly symmetrical as a time average [36]. The possibility of a purely two-dimensional (rotation-symmetric) separation process is considered doubtful by others.
- o The triangular-shaped separation phenomena and the attendant conical compression shocks are generated by the instantaneous separation from one point. The divergence angle of the separation triangle increases in the direction to the nozzle end since the vacuum wall-pressure drops (intensification of the sharp shock-compression).
- o The optical phenomena represent not only the oscillation of the separation point. They are affected by additional influences (and their regularity is enhanced). Condensation and stationary heat transfer to the wall do not set in

instantaneously, rather, they need a certain time (see fig. 11, shifted, slanting compression shock). Therefore the frequencies of the optical phenomena and of the wall-pressure jumps are not the same. The regularity of the separation triangle can be compared with the deformation of a thin-wall nozzle upon separation. The bulging of a nozzle cone illustrated in [44] can generate minor changes in wall contour, similar to the J-2 engine. Such vibrations (waves in a membrane) can explain the periodic sequence of three tepees side-by-side (fig. 46 in [12]).

- o At a fixed combustion-chamber pressure, the position of the first point of pressure increase coincides with the location of the triangular peaks.
- o At a particular combustion-chamber pressure, the lateral forces are very small and the nozzle has full flow (definition of the "separation beginning" is found in sec. 2.4). In spite of this, small separation triangles show up near the nozzle end. With increasing combustion-chamber pressure, these triangles decrease in size in accord with the shift of the point of pressure increase in fig. 7.
- o The optical phenomena extend only up to the turbine inlet since above this, in the direction to the throat, the wall temperature is too high for condensation to occur.
- o The measurements of wall-pressure separation give an average separation behavior which agrees well with the other, larger rocket motors. These were stationary measurements in the J-2S engine with closed turbine inlet openings, extrapolated data of the measurements of the J-2S engine with open Cat Eyes and instationary pressure measurements during the start-up phase of the J-2D engine.
- o The wall-pressure anomalies are probably generated by open turbine-inlet openings since closing the openings nearly confirms the differences between theory and experiment. These phenomena thus should not be considered in investigations of separation.

These findings permit the supposition that the processes observed in the J-2 engine are found in more or less similar, pronounced form, for other rocket engines. Since in these cases an optical observation of the dynamic character of the separation process is not possible (since the exhaust jet is normally not transparent and the wall temperature is not low enough for condensation to occur, and the measurements of wall pressure are normally of low frequency), the J-2 phenomena cannot be determined. But in a chronological average, the J-2 observations agree with the processes described in sec. 2.1 on pure separation.

Thus in an investigation of the separation process, one must always decide whether the dynamic character (side forces) or the quasi-stationary behavior is of interest. The latter permits the design of a nozzle under consideration of flow separation.

### 2.3 Measurement of Separation

To determine the separation behavior of a rocket nozzle, pressure measurements must be used. Optical observations of the exhaust jet can only provide guidelines. In an experiment an attempt is made to measure the pressures  $p_i$  and  $p_p$  as a function of the engine and environmental conditions. Figure 17 shows a photograph of a small rocket motor (4k H<sub>2</sub>/LOX NASA-MSFC engine) with 21 wall-pressure probes.

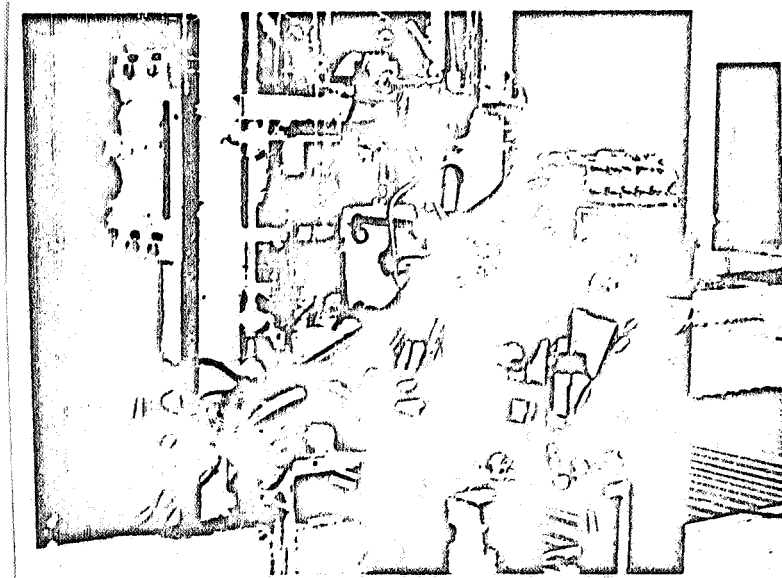


Fig. 17: Test Set-up for Measurement of Separation on the 4k H<sub>2</sub>/LOX Engine of NASA-MSFC.

Experimental data are falsified by measurement error. To determine the wall-pressure profile, only a limited number of pressure probes is available. Therefore, the pressure  $p_i$  at which the first deviation from the vacuum wall-pressure profile occurs, cannot be determined exactly. The same applies to a much greater extent for the plateau pressure. Figure 18 shows different measurements of pressure of the 4k H<sub>2</sub>/LOX engine. The normed pressures during the test without separation show good agreement; the smaller deviations are caused by the accuracy of the probes and amplifier, combustion-chamber pressure error and wall and measurement-hole disturbances. The measurement of wall pressure in the case of separation agrees well with these wall-pressure values, up to the point of separation.

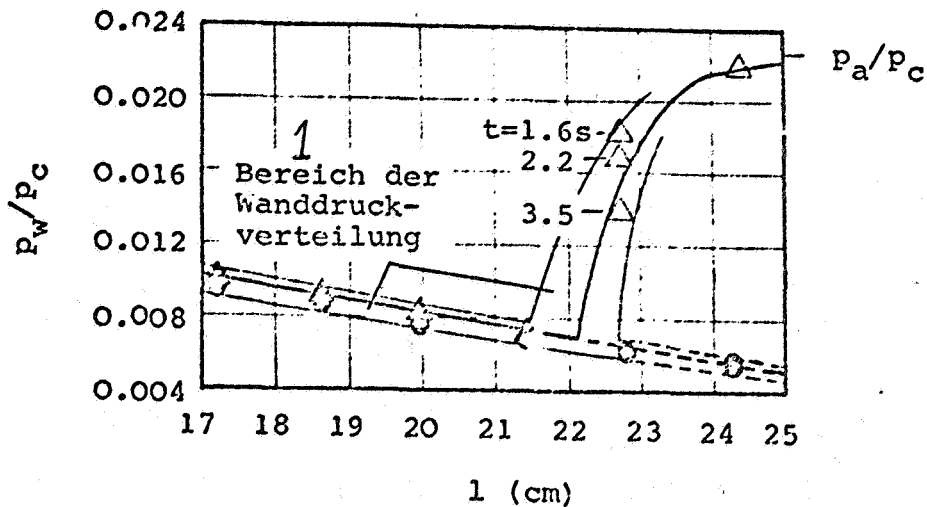


Fig. 18: Wall Pressure Distribution in the 4k H<sub>2</sub>/LOX Engine (NASA-MSFC). Test 268/023 ( $p_c = 42.4$  bar) Test 268/019-022

Key: 1-region of wall-pressure distribution

Between the 4th and 5th measurement point there is the pressure increase; the wall pressure in the separation region also exhibits a dependence on the operating time.

The scattering of pressure data and the limited number of measurement probes permit the entry of a region of possible wall-pressure distribution within which the correct pressure profile must lie. The minimum wall pressure can only be read off to 0.02 bar accuracy; this is about 6% of the absolute value. A determination of the plateau pressure is practically impossible.

This shows that in all flow separation tests on rocket nozzles, the minimum wall pressure  $p_i$  can only be determined within an accuracy of 5 to 10%.\* In many experiments, this value is even exceeded [43]. It is useful to perform a test without separation in order to have a reference pressure distribution which can be used to better determine the minimum point. The plateau pressure is almost impossible to determine.

\*An elegant method of compensating at least in part for the limited number of measurement points, is found in [33]. If the combustion chamber pressure or environmental pressure is quasi-stationary, then by means of the time behavior of the wall pressure it is possible to know when the minimum pressure is reached at a measurement point.

## 2.4 Beginning of Separation

With increasing combustion-chamber pressure or with decreasing environmental pressure, the separation region shifts in the direction of the nozzle end. This relation is shown in fig. 7. In this case the region of back-flow becomes increasingly smaller until finally, the separation zone arrives at the end cross-section. Then the separation point is located in the immediate vicinity of the nozzle end. A slight increase in the pressure ratio leads to a full-flowing nozzle and the separation takes place in the end cross-section. This condition is called the "beginning of separation." It denotes the boundary value from which a flow separation can be expected for a falling pressure ratio. In this case the slanting compression shock arrives near the end cross-section and the minimum pressure is reached before the nozzle end since the compression region is several boundary-layer thicknesses long. If the pressure ratio is increased--proceeding from the beginning of separation--then no qualitative changes take place to the flow and wall-pressure picture. The flow is compressed only in the boundary layer at the nozzle end, without any separation in the actual sense. Since the increase in wall pressure is similar to that of flow separation, this phenomenon is often confused with the actual separation. Thus, this phenomenon is called the "nozzle-end effect" in [29].

To determine the wall pressure at which the beginning flow separation occurs, let us plot the minimum wall pressure against the pressure ratio  $p_c/p_a$ . The measured values of figures 6 and 7 are entered accordingly in fig. 19. With increasing pressure ratio, the minimum wall pressure decreases. This is the region of flow separation in the nozzle. If the separation-region is near the nozzle end, then  $p_i$  obtains a flat minimum. This pressure corresponds to the condition of beginning-separation defined above. Since a larger region of the pressure ratio is overlined where the initial separation pressure is reached, the pressure ratio of beginning separation can hardly be determined with any accuracy from fig. 19. The minimum wall pressure exhibits a hysteresis effect, particularly in the region of beginning separation. It depends on the direction of the combustion-chamber pressure change and is generated by friction, separation and recovery [29, 41]. The above measurement errors are not insignificant and likewise contribute to a band of minimum wall-pressure values. A general statement about the width of this scattering band is not possible (see also 3.1.4). If  $p_c/p_a$  is further increased, then the minimum pressure also increases since no flow separation will occur, until finally, the environmental and nozzle-end pressures coincide.

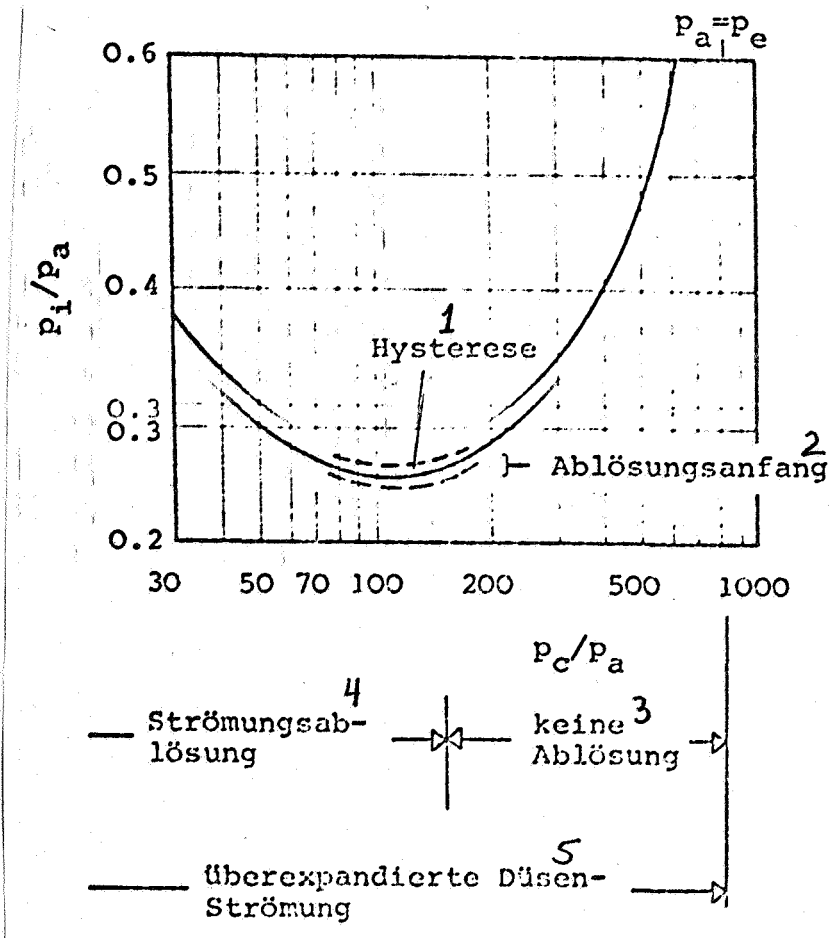


Fig. 19: Minimum Wall Pressure as a Function of the Pressure Ratio (from measurements by [4]).

- Key: 1-hysteresis  
 2-beginning separation  
 3-no separation  
 4-flow separation  
 5-over-expanded nozzle flow

## 2.5 Separation Criterion

An important question in the design of a nozzle is the minimum value of the vacuum nozzle end-pressure  $p_{e\text{vac}}$  at which no flow separation occurs. This value depends on the environmental pressure. With the separation criterion  $K_{sc}$  which describes the condition "no flow separation," we have:

$$p_{e\text{vac}} > p_a K_{sc} \quad (3)$$

$K_{sc}$  depends on the various nozzle parameters. If we know  $K_{sc}$  and the outside pressure, then a nozzle geometry must be chosen which satisfies (3).

The condition "no flow separation" is the boundary case of beginning separation. If the width of the separation region is neglected, then we can write:

$$K_{sc} = \frac{p_i}{p_a} \Big|_{\text{beginning separation}} \quad (4)$$

$K_{sc}$  must be determined by theoretical laws or experimental data. Since in most tests only the minimum wall pressure is determined for several pressure relations and thus the beginning separation is not available, the following simplifying separation criterion must be used:

$$K_{sc} = \frac{p_i}{p_a} \Big|_{\text{separation}} \quad (5)$$

The difference between (4) and (5) is the difference  $p_e - p_p$ , the increase from plateau pressure to the nozzle end-pressure  $p_p$  contained in (5). Since  $p_p$  and  $p_e$  are approximately equal, (5) gives sufficiently accurate values within the range of measurement accuracy.

### 3. Experimental and Theoretical Results of Flow Separation

To design a non-separating nozzle in counter-pressure, the separation criterion is needed. Experimental and theoretical separation data can be used for this. Since all theoretical laws are based on data obtained in tests, one must always rely on the separation experiment.

#### 3.1 Experimental Separation Results

The use of experimental separation results requires the conversion of test data to the desired engine. This leads to several questions: How similar must the engine be in comparison to the new motor so that the data can be applied to real equipment, and what conversion laws must be applied? Therefore, one must know which factors affect the flow separation and what effect they have on the separation criterion. This can only be determined experimentally by comparing the separation results of numerous motors.

##### 3.1.1 Published Experimental Data

Experimental separation data from chemical rocket motors are available from about 14 different places. In table 1 the sources and most important engine parameters are presented. In [35] there is a table of the separation data.

Several comments on table 1 and on the different measurements are needed. In table 1 there are no separation data from engines with solid propellants. Some results are presented in [23].



Since in [23] the measured points are illustrated graphically only and in addition, numerous hot and cold-gas data is also plotted, an identification of the measured points is hardly possible. The data agrees with that of other sources. The measurements of Forster and Cowles and of Bloomer et al. were conducted more than 10 years ago, but they extend over a broad range of test and engine conditions. Thus they belong today to the most important data on separation in chemical engines. There is only a little reliable separation information available on the J-2 engines [12]. Thus the condition "no side forces" is taken together with the combustion chamber and theoretical wall-pressure as a criterion for a full-flow nozzle. Several instationary measurements of wall pressure during the start-up phase of the J-2D engine are available from NASA-MSFC tests. For  $p_i$  the theoretical wall pressure at the point of the first pressure increase is taken, since the measurement of instationary pressure is not very accurate. During the stationary part of the experiments there was good agreement between theoretical and experimental wall pressure. The RL-10 separation data are somewhat questionable, since the measurement lines iced up due to the cryogenic wall cooling. The data of Kah and Lewis with a high-pressure engine are based on short-time tests of about 1 s duration. High-speed photographs show a flow which does not separate until the nozzle end cross-section. In several of the tests of Thayer and Booz with a model rocket motor of the Space Shuttle main engine, separation and recovery occurred. These data differ very much from the other results, so that they should not be used for the specification of a separation criterion.

### 3.1.2 Methods of Graphic Representation

A fundamental question in the evaluation of experimental results is the method of graphic representation. In the case of the flow separation in rocket nozzles, this problem has not been fully solved.

The original method is to use pressure ratios  $p_i/p_a$  and  $p_c/p_a$  [13, 40]. Improvements have been proposed by Green [16] and Schilling [30, 34] in order to reduce the scattering of data in the graphic representation. But the results achieved do not represent an actual improvement since the reduction in scattering is obtained only through a change in scale.

The other method of plotting is based on a result of the separation theories which states that the Mach-number at the beginning of the recompression zone is a decisive parameter for the separation. Therefore in this method,  $p_i/p_a$  is represented as a function of  $M_i$ . This method is also used in the discussion of experimental results.

### 3.1.3 Compilation of the Separation Data on Chemical Rocket Engines

Plotting of the experimental data requires a calculation of the Mach number at point  $i$ . If an isentropic relaxation is assumed along the wall flow-line, then for an ideal gas one can write:

$$M_i = \left\{ \frac{2}{\gamma-1} \left[ \left( \frac{p_c}{p_i} \right)^{\frac{\gamma-1}{\gamma}} - 1 \right] \right\}^{0.5} \quad (6)$$

Since in a real nozzle the isentropic exponent  $\gamma$  changes during the relaxation, the use of a suitable  $\gamma$  is somewhat arbitrary in (6). The occurring errors are not very large since a small deviation from the average isentropic exponent only slightly affects the computed Mach number. The values for the isentropic exponents taken as a basis for the evaluation, are presented in table 2.

Table 2. Isentropic Exponent of the Various Fuel Combinations [3, 42].

Fuel Combination	Isentropic Exponent
HNO <sub>3</sub> /aniline	1.23
H <sub>2</sub> O <sub>2</sub> /benzene	1.20
O <sub>2</sub> /benzene	1.24
O <sub>2</sub> /H <sub>2</sub>	1.26

The separation data of chemical rocket engines are plotted in fig. 20. In addition, the region of cold-gas test data is given; this is compiled in [29] for the values from [1, 5, 11, 25]. The shaded field designates the majority of the cold-gas data. Figure 20 shows that the trend of hot-gas and cold-gas data coincides. With increasing Mach number at the beginning of the recompression zone, the separation pressure decreases. The cold-gas data covers the region of the hot-gas values, but the majority of the cold-gas tests leads to a separation criterion which is about 10% less than that of the hot gas. It is possible that the upper range of cold-gas tests does not represent true separation. This can be a nozzle end-effect as is seen in the data of [1]. Two test series do not agree with the trend of the other hot-gas data. These are the results of tests with small bell nozzles. The observed pressures are much lower than in the other cases.

For an investigation of the influence of different parameters on the separation behavior, a reduction of the scattering in the experimental values is needed. In section 2.3 it was found that

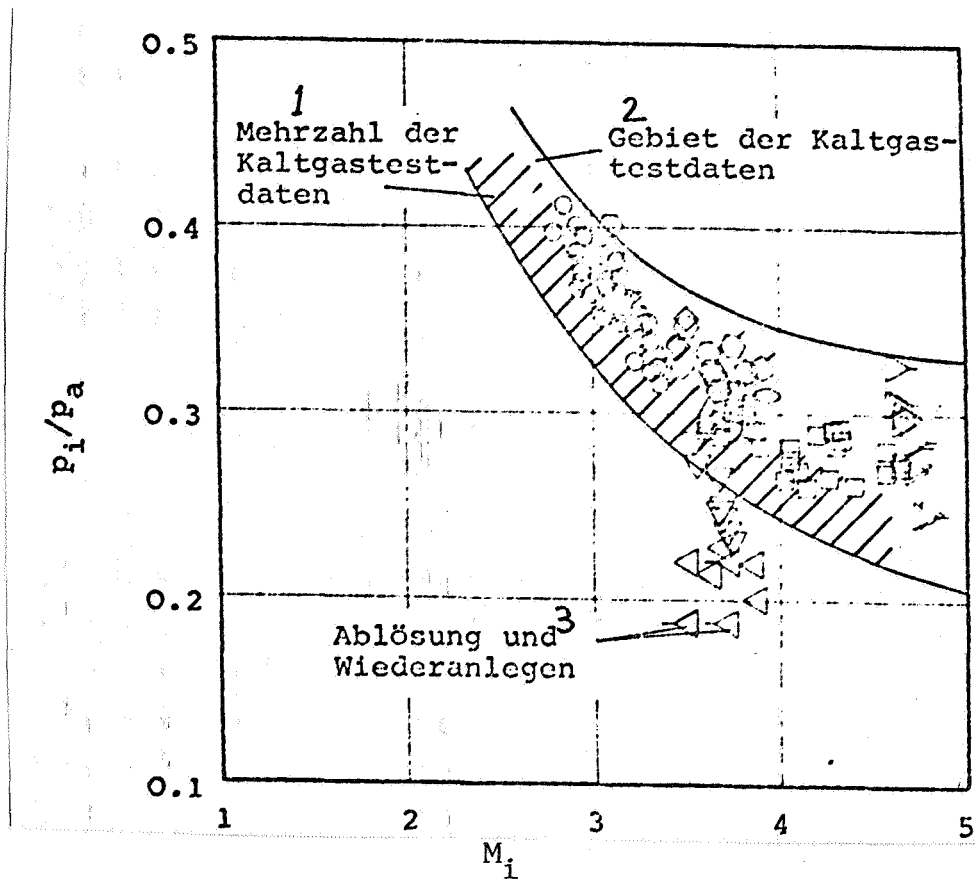


Fig. 20: Compilation of Separation Data in Chemical Rocket Engines [35] (Symbols: See table 1)

Key: 1-majority of cold-gas test data 2-region of cold-gas test data 3-separation and recovery

an error of 5 to 10% must be expected in the separation tests. A usual method for reducing measurement errors is to average different measurements taken under approximately the same conditions. This method can be applied to the separation tests by averaging the data of each engine within a certain region of  $M_i$ . In figure 21 these averaged separation data are presented. The large scattering range of fig. 20 has been reduced dramatically. The separation in chemical rocket engines with higher thrust takes place much earlier than in the small, cold-gas nozzles. The difference is considerable, especially at higher Mach numbers.

### 3.1.4 The Influence of Various Parameters on the Separation Behavior

The averaged separation data of fig. 21 can be used to determine the influence of various parameters on the separation behavior.

With increasing Mach number at the beginning of the recompression zone, the separation criterion declines. At higher Mach numbers, this influence becomes smaller and for very large Mach

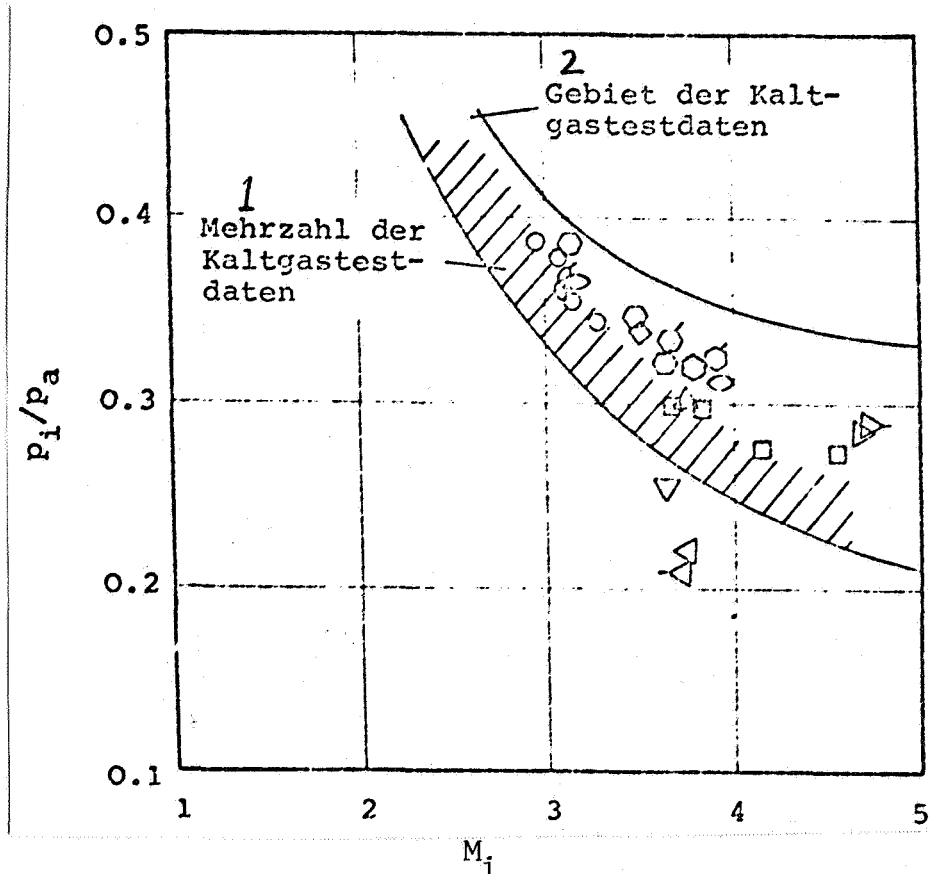


Fig. 21: Average Separation Data of Chemical Engines [35]  
(Symbols: See table 1)

Key: 1-majority of cold-gas test data 2-region of cold-gas test data

numbers,  $p_i/p_a$  certainly will not fall below a certain limit value which is greater than zero. This trend agrees with that of the cold-gas data. The separation values for hydrogen entered in [30] show a separation criterion of 0.2 for a Mach number of 6.2 and this indicates that the lower limit for cold gases lies between 0 and 0.1. In hot-gas tests, this limit can be higher, as we see in fig. 21\*.

The influence of the nozzle angle on the separation point is a question which has been investigated since the beginning of separation measurements. The nearly axis-parallel separation observed in plug nozzles of about  $15^\circ$  half divergence angle, led to the supposition that the separation angle coincides with the divergence angle [33]. The separation pressures of nozzles of different divergence angle are plotted in fig. 22. The available data extends over a region of  $10^\circ$  to  $30^\circ$ . The separation data at a Mach number of about 3...[page 36 is missing]

\*The separation theory of Crocco-Probstein [8] described in sec. 3.3.2 also shows a lower limiting value for  $p_i/p_a$ . For the presented hot-gas data, it lies at 0.12 to 0.19.

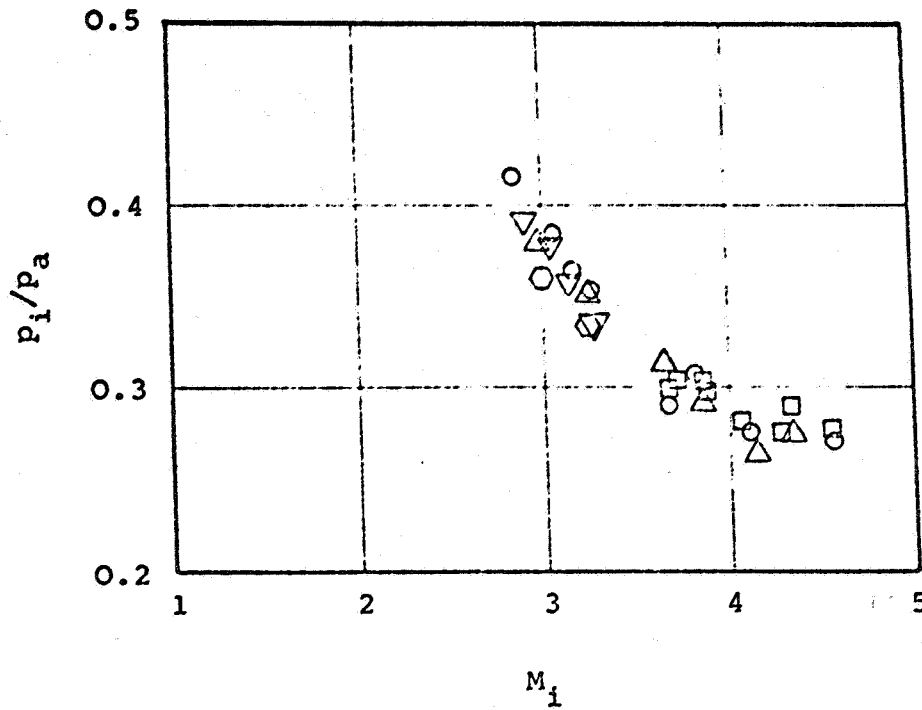


Fig. 22: Separation Point in Plug Nozzles of Different Divergence Angle

Half divergence Angle ( $^\circ$ )	Symbol
10	○
15	▽
20	○
25	□
30	△

at  $10^\circ$ ,  $15^\circ$  and  $20^\circ$ , to have the separation occur later with decreasing angle. The nozzle with  $30^\circ$  does not follow this rule, however. The data at a Mach number of about 4 exhibit no relationship between separation behavior and opening angle. Therefore, one must assume that the separation pressure depends very little or not at all on the nozzle angle. The strong dependence between nozzle angle and separation criterion found by Scheller and Bierlein in [33] is probably the result of a poor pressure measurement since the computed, two-dimensional value does not agree with the measured values.

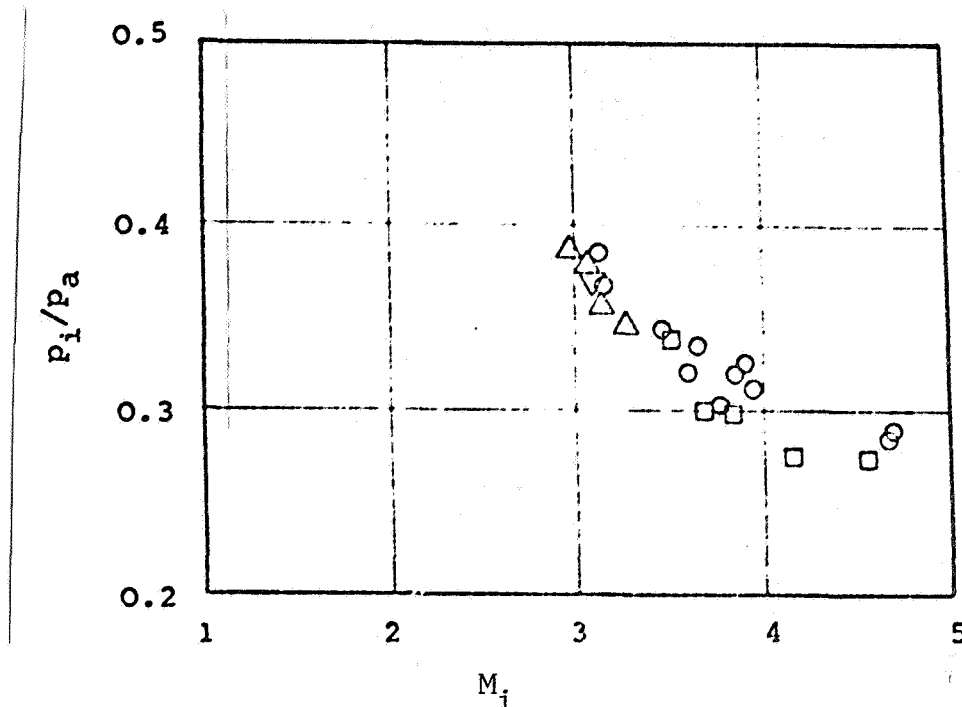


Fig. 23: The Influence of the Isentropic Exponents on the Separation Point [35].

Fuel Combination	Symbol
$HNO_3$ /aniline	$\circ$
$H_2O_2$ /benzine	$\diamond$
$O_2$ /benzine	$\square$
$O_2$ / $H_2$	$\Delta$

In separation tests with different fuel combinations, the isentropy exponent varies. Figure 23 shows the separation pressure of the averaged tests of fig. 21 and the points corresponding to the particular  $\gamma$  are marked. It is visible that a negligible effect is present.

Other parameters like wall configuration--smooth wall or tube construction--and wall temperature have no significant influence on the separation behavior within the scattering of measured values [35].

Figure 21 shows that there is a difference between the separation data of chemical engines and that of the cold-gas tests. There is also a certain scattering of the averaged data of chemical engines; this is particularly striking in the measured values of rocket engines in the range of  $M_i = 3.7$ . This data is plotted in fig. 24 against the thrust of the engines. With increasing thrust, the separation pressure increases in the bell nozzle until it approximately equals that of the larger plug nozzles.

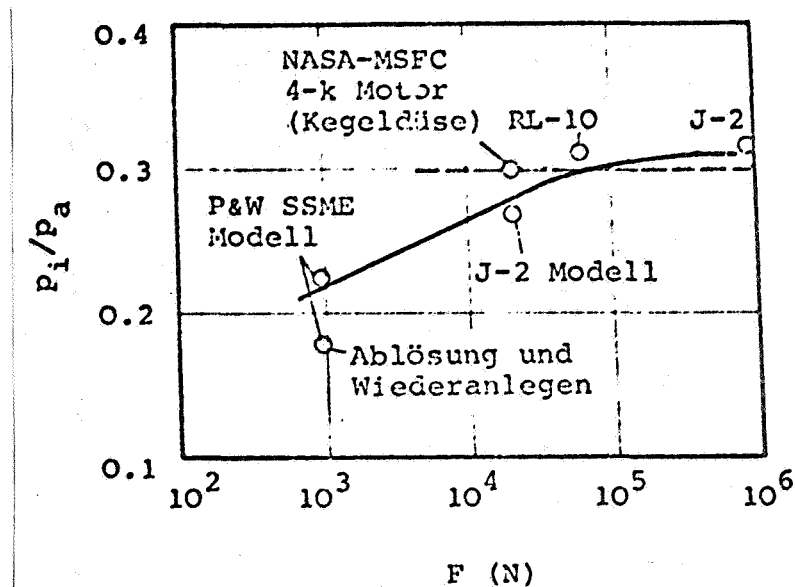


Fig. 24: Separation Pressure of Engines with Bell Nozzles having Different Thrust Values ( $M_1 \approx 3.7$ , LOX/H<sub>2</sub>)

A final explanation of this effect is not possible since the number of corresponding test values is still much too small. Besides the measurement errors which can cause only a part of the scattering, the following additional items may be responsible for this behavior:

-Reynolds number

In fig. 24 a Reynolds number effect could be supposed, since with increasing thrust, the Re-number increases along the wall. But in all turbulent separation measurements, little or no Re-effect is found [10, 24]. Since the separation process takes place within a very short distance and thus almost exclusively the pressure-pulse forces are decisive (see sec. 3.3.2), the viscosity forces have only an insignificant influence.

-Development of Boundary Layer

The boundary layer forms in a curved nozzle due to the pressure distribution and it forms perpendicular to the nozzle wall, in contrast to the process in a plug nozzle. Thus, the separation behavior can be affected (see Crocco-Probstein theory in sec. 3.3.2). In addition, in a small nozzle the boundary layer takes up relatively more space than in a large engine, so that three-dimensional effects can play a role.

-Change of Separation Length (Oscillation Width of the Separation Region) due to the Test and Engine Conditions

The average separation process takes place within a certain distance which amounts to several thicknesses of the boundary layer. The length of this zone can be affected by the engine

operating conditions and the test conditions. Model tests with cold-gas nozzles and small engines can be conducted very carefully (rigid model, smooth-polished wall). In these cases the separation length is shorter (lower separation oscillations [36]) and consequently there results a flow separation at smaller pressures than in a large engine where the disturbances of the boundary layer and inflow conditions are more severe. Due to these disruptions, the flow separates even at a higher pressure.

The latter phenomenon would mean that besides a general trend of the separation pressure with the Mach number, the exact values depend on the particular engine and test conditions. The measured results presented in [36] make this influence appear possible. The separation data of larger engines accordingly represent a type of upper limit which can only be undercut in very carefully performed tests with the appropriate model engines. Model tests are thus useless for the determination of the separation behavior of large engines (see fig. 24, J-2 model and large engine).

### 3.1.5 Summary of Experimental Separation Results

The various experimental investigations of flow separation in supersonic nozzles turned up a series of (partly scattered) effects which can be combined into the following findings:

- o The separation criterion  $p_i/p_a$  is lowered with increasing Mach number  $M_i$  of the first recompression point.
- o There probably exists a lower limit for this "separation pressure" which could lie between 0.1 and 0.2  $p_a$  for hot-gas engines.
- o The separation criteria of large engines (bell and plug nozzles) are higher than those of cold-gas and hot-gas model engines. The measured data of larger engines represents a type of upper separation limit.
- o The separation criterion is affected slightly or not at all by:
  - o Nozzle divergence angle
  - o Nozzle contour (plug or bell nozzle)
  - o Wall contour
  - o Wall temperature
  - o Fuel combination

### 3.2 Experimental Separation Criteria

For the design of a nozzle it is useful to have an analytical relation for the separation criterion, instead of having to read off the pertinent value from fig. 21. The usual method is to

use an empirical function whose constants are determined by the data points.

Several empirical separation criteria have been published, all of which provide a relationship between the separation pressure and the pressure ratio  $p_c/p_a$ .

Summerfield [40]:

The oldest separation criterion comes from M. Summerfield. Building on the tests of Forster and Cowles, the following expression results as a guideline value for low pressure conditions ( $p_c/p_a \approx 15$  to 20):

$$\left| \frac{p_i}{p_a} = 0.4 \right. \quad (7)$$

At higher pressure conditions, this value decreases.

Schilling [30, 34]:

Building on the Green method [16] of norming of  $p_i$  with the combustion chamber pressure instead of  $p_i/p_a$ , Schilling provides an expression:

$$\left| \frac{p_i}{p_c} = 0.583 \left( \frac{p_c}{p_a} \right)^{-1.195} \right. \quad (8)$$

Equation (8) applies for short, bell nozzles [1]. Similar equations can be set up for long bell nozzles and plug nozzles. If equation (8) is multiplied by  $p_c/p_a$ , then the separation criterion results as:

$$\left| \frac{p_i}{p_a} = 0.583 \left( \frac{p_c}{p_a} \right)^{-0.195} \right. \quad (9)$$

A comparison of equation (9) with the averaged experimental data of fig. 21 shows that the Schilling equation provides far too small separation pressures. Thus one must assume that (8) is based on cold-gas data. Equation (9) should therefore not be taken as a separation criterion for chemical engines [35].

Kalt-Bendall [23]:

S. Kalt and D. Bendall apply an equation similar to (9). The test values of cold-gas nozzles and rocket engines with solid and liquid propellants of differing sizes led to the relation:

$$\left| \frac{p_i}{p_a} = 0.667 \left( \frac{p_c}{p_a} \right)^{-0.2} \right. \quad (10)$$

At low pressure relationships the agreement with averaged data of fig. 21 is relatively good; but at greater Mach numbers, (10) like (9), deviates from the experimental data.

All equations with a simple power law for the pressure relation decrease too much at higher Mach numbers of the separation pressure. More complicated equations for the pressure relation like that in [30], can indeed improve the agreement with experimental data within a broader range of the pressure ratio, but a significant influence of the isentropy exponent on the separation pressure remains, and this was not observed in the test. The preparation of an empirical separation equation with the pressure ratio is thus connected with an "a priori" specified isentropy exponent.

In an empirical equation it is better to take the Mach number  $M_i$  from the beginning of the separation zone, instead of the pressure relationship  $p_c/p_a$ . An example for one such separation criterion (presented in fig. 25 together with the averaged experimental data) runs:

$$\frac{p_i}{p_a} = (1.88 M_i - 1)^{-0.64} \quad (11)$$

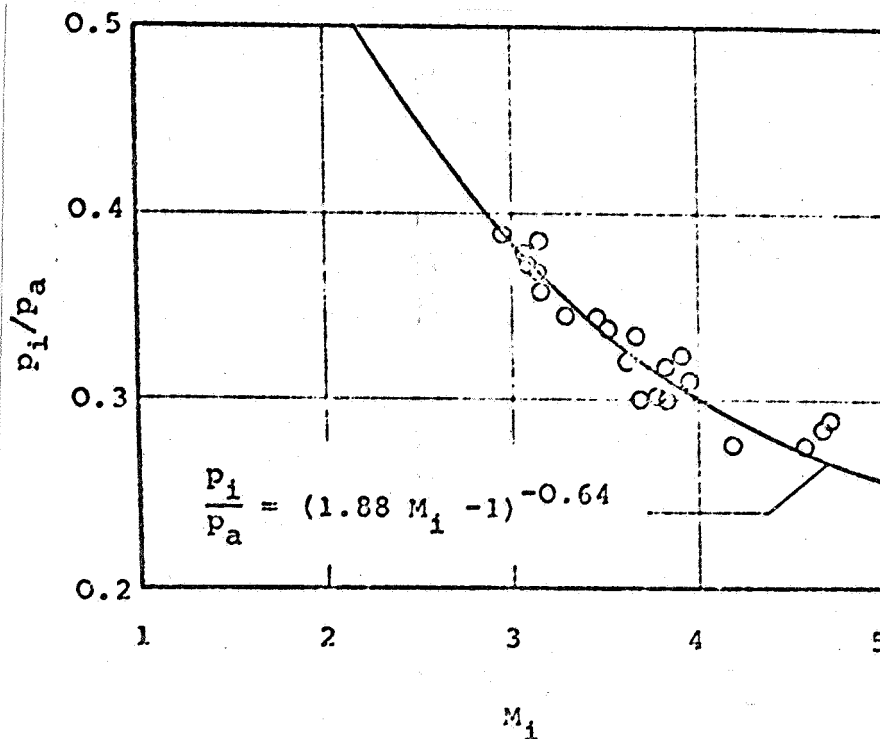


Fig. 25: Empirical Separation Criterion (o : Averaged Separation Data of Chemical Engines)

For  $M_i$  the value '5' should not be exceeded since test values above this range are not available.

### 3.3 Theoretical Calculation of the Separation

The phenomenon of separation of turbulent boundary layers at supersonic speed can occur not only in over-expanded rocket nozzles, but also when flowing over steps, around wedges and in the interaction between incident compression shocks and boundary layers. The theories proposed to account for this have thus also been applied in part to flow separation in nozzles.

#### 3.3.1 Overview of the Most Important Flow Separation Theories for Rocket Nozzles

The task of the flow separation theory consists in describing the change in the boundary layer during the recompression and its interplay with the outlet flow. The methods developed for this calculation sometimes differ significantly; they are based on the following points:

- o Equilibrium between wall friction and pressure change in the separation region (Donaldson-Lange [9])
- o Pulse change of the boundary layer in the separation region and characteristic velocity profile for the points  $i$  and  $s$  (Tyler-Shapiro [46]). (A principally similar method is used by J. Nielsen, J. Nielsen Engineering & Research, Inc., for the calculations in the SQID project)
- o Pulse change of the boundary layer in the separation region, transformation in the incompressible form and boundary-layer form factors (Crocco-Probstein [8])
- o Constant ratio of Mach numbers before and after the separation point (Mager [28], Guman [18], Reshotko-Tucker [32]\*, Lawrence [25])
- o Pressure change in the boundary layer and rotation of the outward flow (Mager [28])
- o Similarity of the separation pressure-increase (Chapman [6])
- o Characteristic flow line in the boundary layer (Gadd [15], Arens-Spiegler [2]).

---

\*Reshotko-Tucker, Lawrence and Tyler-Shapiro do not make a distinction between the separation point and plateau pressure-point.

Although several of these theories are old, they are still used today in the calculation of flow separation in rocket nozzles [29].

In [35] the various theories are presented and compared with experimental data. It turns out that the calculation method of L. Crocco and R. Probstein gives the best agreement with the experimental data. In the other theories, either the isentropy exponent will have a strong influence on the separation pressure [2, 6, 15, 18, 28, 32] or the Reynolds number formed with the local nozzle length, will play an important role [6, 9]. The theory of [46] even gives a rising separation pressure at higher Mach numbers.

### 3.3.2 Separation Theory of L. Crocco and R. Probstein [8]

The boundary-layer model of L. Crocco and R. Probstein to compute the separation pressure is presented in figure 26. At that point where the slanting compression shock exits from the boundary layer, the outflow is diverted. Near the separation point the usual assumptions of boundary-layer theory are not applicable since the pressure distribution perpendicular to the boundary layer is not constant. These deviations from the constant pressure distribution decline quickly both upstream and downstream, so that at points *i* and *p*, a constant pressure can be expected. The distance between *i* and *p* amounts to only a few boundary-layer thicknesses. Thus the mass inflow into the boundary layer and the wall friction can be neglected.

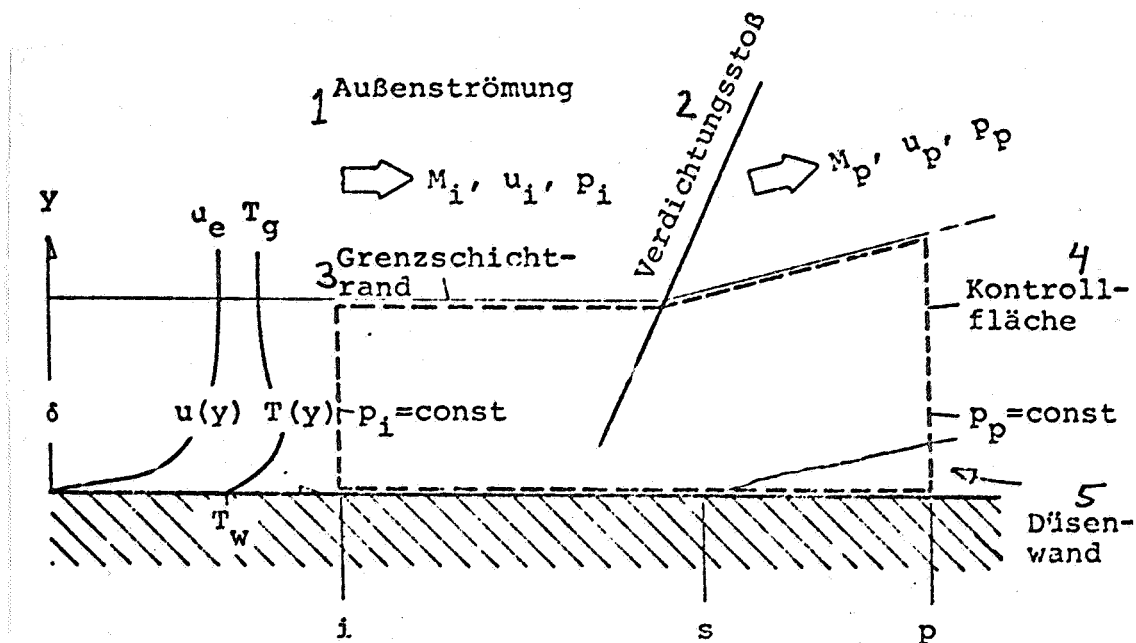


Fig. 26: Boundary-Layer Model of the Crocco-Probstein Separation Zone [8]

Key: 1-outward flow 2-compression shock 3-edge of boundary layer  
4-control surface 5-nozzle wall

With the compression thickness  $\delta^*$  [44]

$$\delta^* = \int_0^{\delta} \left(1 - \frac{\rho u}{\rho_e u_e}\right) dy \quad (12)$$

and the pulse-loss thickness  $\theta$

$$\theta = \int_0^{\delta} \frac{\rho u}{\rho_e u_e} \left(1 - \frac{u}{u_e}\right) dy \quad (13)$$

one can write the following expression for the mass flow  $\dot{m}$  and the pulse flow  $\dot{I}$ :

$$\dot{m} = \rho_e u_e \delta \left(1 - \frac{\delta^*}{\delta}\right) \quad (14)$$

$$\dot{I} = \rho_e u_e^2 \delta \left(1 - \frac{\delta^*}{\delta} - \frac{\theta}{\delta}\right) \quad (15)$$

In this case,  $\rho$  denotes the density and  $u$  the velocity in the boundary layer,  $e$  stands for the values at the edge of the boundary layer.

If we consider only time-averaged processes and select a control volume as is illustrated in fig. 26, then the laws of conservation become:

$$\dot{m}_i = \dot{m}_p \quad (16)$$

$$\dot{I}_i - \dot{I}_p = \delta_i (p_p - p_i) \quad (17)$$

The change in flow values at the edge of the boundary layer due to the slanting compression shock is described by the Hugoniot-Rankine equation:

$$\frac{T_p}{T_i} = \frac{\frac{\gamma+1}{\gamma-1} + \frac{p_p}{p_i}}{\frac{\gamma+1}{\gamma-1} + \frac{p_i}{p_p}} \quad (18)$$

where  $T$  is the temperature at the edge of the boundary layer and  $\gamma$  is the isentropy exponent.

If we transform (14) and (15) in accord with the Crocco-Lees theory [7] and combine (16) to (18), then we obtain:

$$\frac{p_p - p_i}{2\gamma} \left[ K_{CL1_i} M_i^{-2} + \frac{\gamma-1}{2} (K_{CL1_i} - 1) \right] = \quad (19)$$

$$1 - \frac{K_{CL2_p}}{K_{CL2_i}} \left( \frac{2}{\gamma-1} \right)^{0.5} M_i^{-1} \left[ 1 + \frac{\gamma-1}{2} M_i^2 \frac{\frac{\gamma+1}{\gamma-1} + \frac{p_p}{p_i}}{\frac{\gamma+1}{\gamma-1} + \frac{p_i}{p_p}} \right]^{0.5}$$

The constants  $K_{CL}$  result from the transformed compression and pulse-loss thicknesses as:

$$K_{CL1} = \frac{1}{1 - \frac{\delta^*}{\delta} - \frac{\theta}{\delta}} \quad \text{incompressible} \quad (20a)$$

$$K_{CL2} = \frac{1}{K_{CL1}} \frac{1}{1 - \frac{\delta^*}{\delta}} \quad \text{incompressible} \quad (20b)$$

In equation (19) the pressure increase for a given Mach number  $M_i$  depends only on the boundary-layer values before and after the separation region. If we solve (19) for the Mach number, then we find:

$$M_i^2 = \frac{1}{2 \left[ K_{CP1}^2 - \left( \frac{K_{CL2_p}}{K_{CL2_i}} \right)^2 \right]} \left[ K_{CP2}^2 + K_{CP1} K_{CP2} + \left( K_{CP2} (K_{CP2} + 2K_{CP1} K_{CP2}) + \left( \frac{K_{CL2_p}}{K_{CL2_i}} \right)^2 K_{CP3}^2 \right)^{0.5} \right] \quad (21)$$

where

$$K_{CP1} = 1 - \frac{\gamma-1}{2} \left( \frac{p_p}{p_i} - 1 \right) (K_{CL1_i} - 1) \quad (22a)$$

$$K_{CP2} = \frac{2}{\gamma-1} \left( \frac{K_{CL2p}}{K_{CL2i}} \right)^2 \frac{\frac{P_i}{P_p} - \frac{P_p}{P_i}}{\frac{\gamma+1}{\gamma-1} + \frac{P_i}{P_p}} \quad (22b)$$

$$K_{CP3} = \frac{2}{\gamma} K_{CL1i} \left( \frac{P_p}{P_i} - 1 \right) \quad (22c)$$

The functional relationship of equations (21) and (22) is illustrated in figure 27. The values selected for  $K_{CL}$  lead to good agreement between theoretical and experimental separation data. The influence of the isentropy exponent on the separation behavior is rather small—a phenomenon which agrees well with the experiment.

This separation theory shows that the pressure at which the flow separation occurs in the nozzle, depends on the boundary-layer parameters of compression thickness and pulse loss thickness. Disturbances in boundary layer development due to wall oscillations, pressure fluctuations and surface roughness change the Crocco-Lees parameters and the separation occurs at a different pressure.

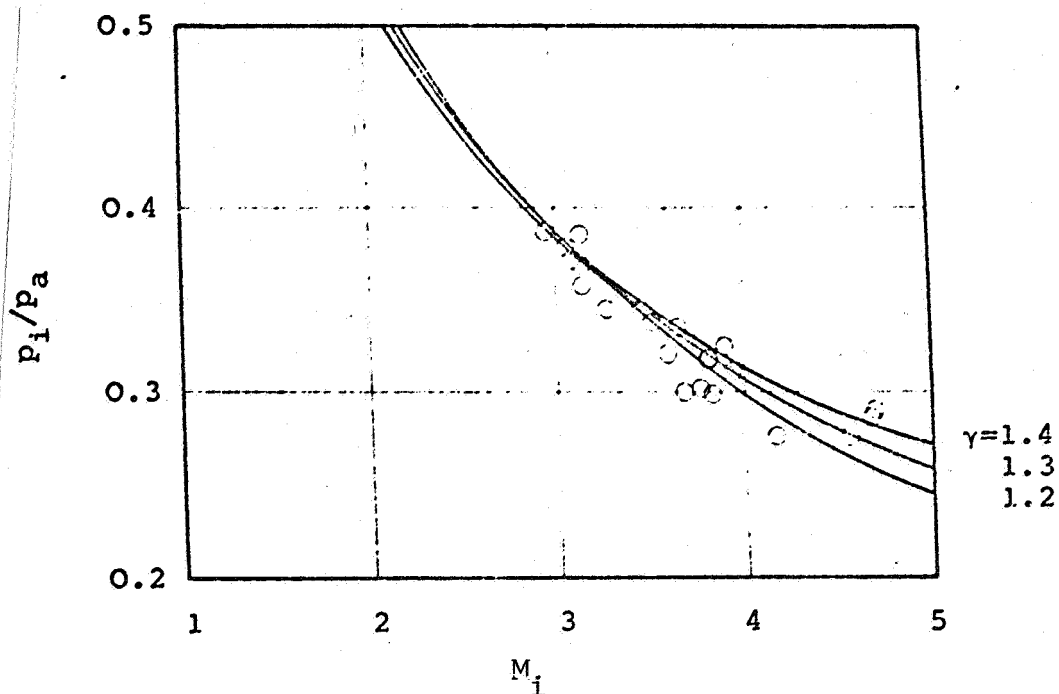


Fig. 27: Separation Criterion of Crocco-Probstein

$$K_{CL1i} = 1.4; \quad K_{CL2p} / K_{CL2i} = 0.865.$$

o Averaged experimental data

## REFERENCES

- [1] Ahlberg, J.H. | et al. : Truncated perfect nozzles in optimum nozzle design. In: ARS-Journal Vol. 31, No. 5 (May 1961), p.614-620
- [2] Arens, M., E. Spiegler: Shock induced boundary layer separation in overexpanded conical exhaust nozzles. In: AIAA-Journal Vol. 1, No. 3 (March 1963), p.578-581
- [3] Barrere, M. | et al. : Rocket propulsion. Elsevier Publishing Company New York, 1961
- [4] Bloomer, H.J., R.J. Antl, P.E. Renas: Experimental study of effects of geometric variables on performance of conical rocket engine exhaust nozzles. NASA TN D-846 (1961)
- [5] Campbell, C.E., J.M. Farley: Performance of several conical convergent-divergent rocket type exhaust nozzles. NASA TN D-467 (1961)
- [6] Chapman, D.R., D.M. Kuehn, H.K. Larson: Investigation of separated flows in supersonic and subsonic streams with emphasis on effect of transition. NACA TN 3869 (1957)
- [7] Crocco, L., L. Lees: A mixing theory for the interaction between dissipative flows and nearly isentropic streams. In: Journal of the Aeronautical Sciences Vol. 19, No. 10 (Oct. 1952), p.649-676
- [8] Crocco, L., R.F. Probstein: The peak pressure rise across an oblique shock emerging from a turbulent boundary layer over a plane surface. Princeton University Report 254 (March 1954)
- [9] Donaldson, C. du, R.H. Lange: Study of pressure rise across shock waves required to separate laminar and turbulent boundary layers. NACA TN 2770 (1953)
- [10] Elkstroem, A.: Incipient separation at supersonic and hypersonic speeds. University of Tennessee, Space Institute (Tullahoma), Short Course on Flow Separation (Nov. 1972)
- [11] Farley, J.M., C.E. Campbell: Performance of several method of characteristics exhaust nozzles. NASA TN D-293 (1960)
- [12] Fenwick, J., M. Moriarty, L. Nave, A. Petersen: Test results and analyses of J-2S engine side load program. Rocketdyne Division, NAR, Report CDR 3124-4087 (April 27, 1973)

- [13] Forster, C.R., F.B. Cowles: Experimental study of gas-flow separation in overexpanded exhaust nozzles for rocket motors. JPL-Progress Report No. 4-103 (1949)
- [14] Fuller, P.N.: J-2S nozzle side load study. Final Report. Rocketdyne Division, NAR, Report R-9045 (August 1, 1972)
- [15] Gadd, G.E.: Interactions between wholly laminar and wholly turbulent boundary layers and shock waves strong enough to cause separation. In: Journal of the Aeronautical Sciences Vol. 20, No. 11 (Nov. 1953), p.729-739
- [16] Green, L.jr.: Flow separation in rocket nozzles. In: ARS-Journal Vol. 23, No. 1 (Jan-Feb 1953), p.34-35
- [17] Gross, K.W.: Unpublished Boundary Layer Data of the SSME (NASA-MSFC-S&E-ASTN-PP) (Jan. 1973)
- [18] Guman, W.J.: On the plateau and peak pressure of regions of pure laminar and fully turbulent separation in two dimensional flow. In: Journal of the Aeronautical Sciences Vol. 26, No. 1 (Jan. 1959), p.56
- [19] Hege, D.W.: Semi-Annual Technical Program Report, Atlas. Rocketdyne Division, NAA, Report R-354-IP (AFO4(645)-1), (Dec. 30, 1956)
- [20] Herbert, M.V., R.J. Herd: Boundary layer separation in supersonic propelling nozzles. Ministry of Aviation, Reports and Memoranda No. 3421 (1964)
- [21] Kah, C.L., G.D. Lewis: High pressure engine feasibility program. Pratt&Withney Aircraft, FR-1171 (Dec. 10, 1964)
- [22] Kah, C.L., G.D. Lewis: High chamber pressure staged combustion research program. Final report. Pratt&Withney Aircraft, FR-1676 (June 30, 1966)
- [23] Kalt, S., D. Bendal: Conical rocket performance under flow separated conditions. In: Journal of Spacecrafts and Rockets Vol. 2, No. 3 (May 1965) p.447-449
- [24] Lange, R.H.: Present status of information relative to the prediction of shock induced boundary layer separation. NACA TN 3065 (1955)
- [25] Lawrence, R.A.: Symmetrical and unsymmetrical flow separation in supersonic nozzles. Southern Methodist University Texas, Ph. D. Thesis 1967
- [26] Lewis, J.T.: Results of separated nozzle flow studies on E-6 and E-7 engine stands. Pratt&Withney Aircraft, SMR FR- (Febr. 8, 1967)
- [27] Lombardo, J., K.W.Gross, S. Omori: Analytical prediction of the ice formation inside the J-2 engine nozzle contour (200k thrust level). NASA-MSFC Internal Memorandum to H.G. Paul (S&E-ASTN-PP) (71-M-163)

- [28] Mager, A.: On the model of the free, shock separated turbulent boundary layer. In: Journal of the Aeronautical Sciences Vol. 23, No. 2 (Febr. 1956) p.181-184
- [29] Nave, L.: Evaluation of the nozzle incipient separation chamber pressure for the SSME 470 k engine. Rocketdyne Division, NAR, Report (Dec. 1, 1972)
- [30] Pratt&Withney Aircraft: Suggested program for applied research on nozzle flow separation. Pratt&Withney Aircraft, FP 65-117 (1966)
- [31] Rocketdyne: Analysis of predicted side loads in the nozzle of the space shuttle booster and orbiter main engine. Rocketdyne Division, NAR, Report SSE 4.1.1 D-1414-2 (1970)
- [32] Reshotko, E., M. Tucker: Effect of a discontinuity on turbulent boundary layer thickness parameters and application to shock-induced separation. NACA TN 3454 (1955)
- [33] Scheller, K., J.A. Bierlein: Some experiments on flow separation in rocket nozzles. In: ARS-Journal Vol. 23 (1953) p.28-32
- [34] Schilling, T.W.: Flow separation in a rocket nozzle. University of Buffalo, M.S. Thesis (June 1962)
- [35] Schmucker, R.H.: Status of flow separation prediction in liquid propellant rocket engines. George C. Marshall Space Flight Center NASA TMX (im Druck)
- [36] Schmucker, R.H.: Flow Processes in Overexpanded Chemical Rocket Nozzles. Part 2: Lateral Forces due to Asymmetrical Separation. Lehrstuhl für Raumfahrttechnik, TU Munich, TB-10 (in preparation)
- [37] Shapiro, A.H.: The dynamics and thermodynamics of compressible fluid flow. Vol. 1 and 2, The Ronald Press Company, New York (1954)
- [38] Stodola, A.: Steam and gas turbines. Mac Graw-Hill Book Company, New York (1927)
- [39] Stromsta, R.R.: Results of J-2SE 40:1 area-ratio bell nozzle design and cold flow test program. Rocketdyne Division, NAR, Report LAP 67-368 (RC) (Aug. 31, 1967)
- [40] Summerfield, M., C. Forster, W. Swan: Flow separation in overexpanded supersonic exhaust nozzles. In: Jet propulsion Vol. 24, No. 9 (Sept. 1954) p.319-320
- [41] Sunley, H.L., V.N. Ferriman: Jet separation in conical nozzles. In: Journal of the Royal Aeronautical Society Vol. 68 (1964) p.808-817
- [42] Sutton, G.P.: Rocket propulsion elements. John Wiley and Sons, New York (1967)

- [43] Thayer, E.B., D.E. Booz: Flow Separation Tests of Candidate Space Shuttle Nozzles. Pratt&Withney Aircraft SMR, FR-3491 (Nov. 21, 1969)
- [44] Truckenbrodt, E.: Flow Mechanics. Springer Pub. Berlin, 1968
- [45] Tuovila, W.J., N.S. Land: Experimental Study of Aeroelastic Instability of Overexpanded Rocket Nozzle Extension. NASA TN D-4471 (April 1968)
- [46] Tyler, R.D., A.H. Shapiro: Pressure Rise Required for Separation in Interaction between Turbulent Boundary Layer and Shock Wave. In: Journal of the Aeronautical Sciences, Vol. 20, No. 12 (Dec. 1953) pp. 858-860

APPENDIX: Prediction of Separation for the Space Shuttle Main Engine

In fig. A1 the normed wall-pressure distribution is illustrated in the nozzle of the Space Shuttle Main Engine. With the vacuum pressure ratio at the nozzle end  $p_e/p_c$  the following expressions result via equations (6) and (11):

$$M_i = 4.5 \quad (\gamma = 1.26) \quad (\text{Multi-dimensional value from [17]})$$

$$M_i = 4.2$$

$$p_i/p_a = 0.28 \text{ to } 0.29 \quad (\text{the upper value takes into account the scattering of experimental data})$$

Thus, for the pressure ratio at which the nozzle will have full flow:

$$\left. \begin{array}{l} p_c/p_a \\ \text{beginning} \\ \text{separation} \end{array} \right\} = 148 \text{ to } 153$$

and the upper value should be taken for safety reasons.

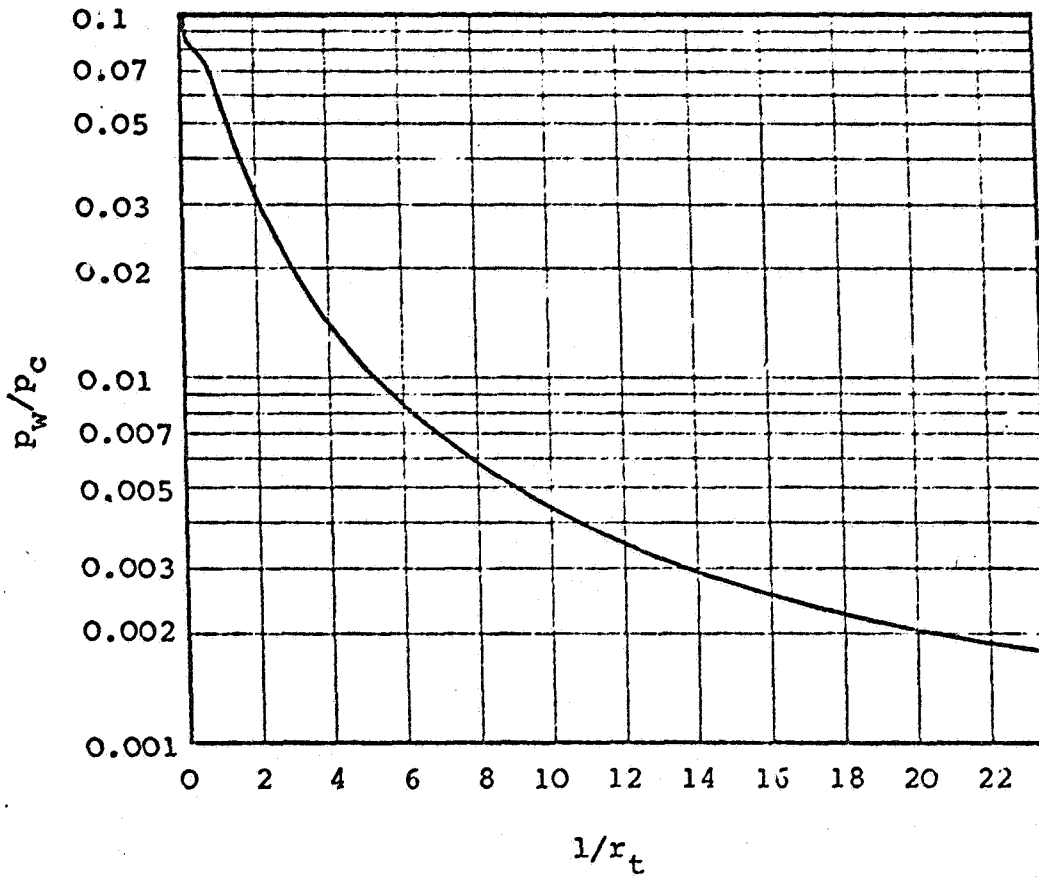


Fig. A1: Normed Wall-Pressure-Distribution of the Space Shuttle Main Engine [17]